Modulation-Level Coding for Wireless Network Coding

by

Ibrahim M. Al-Solami

A thesis
presented to the University of Waterloo
in fulfillment of the
thesis requirement for the degree of
Master of Applied Science
in
Electrical and Computer Engineering

Waterloo, Ontario, Canada, 2009

I hereby declare that I am the sole author of this thesis. This is a true copy of the thesis, including any required final revisions, as accepted by my examiners.

I understand that my thesis may be made electronically available to the public.

Ibrahim M. Al-Solami

Abstract

When intermediate nodes encode messages in wireless network coding, a question arises: Which modulation scheme should be used to broadcast the encoded message? Should it be limited to a receiver with a low modulation-level requirement to maintain an acceptable BER or should it be broadcasted at the desired modulation-level of a receiver with a higher rate requirement? Such conflicting requirements typically arise when one receiver has a low channel capacity while the other has a higher one.

Recently, the deployment of network coding in wireless networks has attracted significant research attention, mainly due to the capability of network coding to improve throughput and save energy. However, a challenging problem in wireless network coding is to determine which modulation scheme to employ in the broadcast phase when receivers have diverse modulation scheme requirements, e.g., Node A may desire an 8-PSK modulation scheme on the broadcasted signal, while Node B may require a QPSK on the same broadcasted signal.

In this thesis, we introduce a new coding scheme aimed at solving the diverse modulation problem. The scheme is based on coding information such that a receiver with a high modulation-level requirement can decode more information from a broadcasted signal than a receiver with a low one. Several codes have been designed for various combinations of modulation schemes. Analytical studies have been carried out to quantify the performance of the proposed scheme. Extensive simulations have been conducted to demonstrate the performance of the proposed scheme and validate the accuracy of our analytic model.

Acknowledgements

I arrived here at Waterloo two years ago and it has been an enjoyable journey ever since. There are a number of people that I would like to thank for this.

I would like to thank my dear Mother Aziza Alharbi, Father Mohammed Alsolami, Sister Sana Alsolami, and Brother Walid Alsolami for their love, caring, and prayers. They have sacrificed a lot for me throughout the years.

My sincere appreciation goes to my supervisors Professor Xuemin (Sherman) Shen and Professor Zhou Wang for their valuable insights, enthusiasm, and guidance during the course of my studies.

I am really grateful to Professor Shen. He has always shared with me his academic and personal experience. His outstanding commitment has made him a very successful researcher. It is a great honor to be his student.

I am sincerely indebt to Professor Wang. I still remember the time when he would continuously encourage me during the hard times of my research. His exceptional dedication has made him a very successful professor. I am extremely glad that he is my supervisor.

I would also like to thank Professor En-hui Yang and Professor Mohamed Oussama Damen for serving as members of my thesis committee; their efforts and valuable comments on this thesis are greatly appreciated.

Special thanks to the Saudi Arabian Ministry of Higher Education for giving me a scholarship to pursue my Master's degree. I would also like to thank Saudi Arabian Cultural Bureau in Canada for their support.

I would like to express my gratitude to members of the broadband communication research (BBCR) lab for the valuable thoughts we shared together in our group meetings; I am extremely blessed to have worked with such professional people.

Fortunately, I have meet a number of people who have made Waterloo feel like home, namely: Deniz Rahimi, Samin Barakati, Babak Alavikia, Fariborz Rahimi, Khaled Almotairi, Khalid Alsubhi, Maazen Alsabaan, Masoud Barakati, Mehri Mehrjoo, Rashin Salehi, Suhail Al-Dharrab, and Zeyad Almutairi.

Ibrahim M. Al-Solami

University of Waterloo
Waterloo, Ontario, Canada
November 1, 2009

Dedication

This thesis is dedicated to
my dear Mother, Father, Sister, and Brother.

Contents

List of Figures

List of Abbreviations

AWGN	Additive White Gaussian Noise
BER	Bit-Error Rate
BPSK	Binary Phase-Shift Keying
dB	Decibel
FSK	Frequency-Shift Keying
ML	Maximum-Likelihood
M-PSK	M-ary Phase-Shift Keying
M-QAM	M-ary Quadrature Amplitude Modulation
PSK	Phase-Shift Keying
QAM	Quadrature Amplitude Modulation
QPSK	Quadrature Phase-Shift Keying
SNR	Signal-to-Noise Ratio
VANET	Vehicular Ad-hoc Network
WBAN	Wireless Body Area Network
WiFi	Wireless Fidelity
WiMAX	Worldwide Interoperability for Microwave Access
WSN	Wireless Sensor Network

List of Symbols and Notations

$\|\mathbf{x}\|$	The Euclidean norm of vector $\mathbf{x}$
a^j	The jth bit in a n-tuple
$\boldsymbol{\alpha}$	Binary sequence of Node A
b^j	The jth bit in a m-tuple
$\boldsymbol{\beta}$	Binary sequence of Node B
$\mathbb{C}$	The set of complex numbers
$\mathbf{C}$	Codebook
C_i	Codeword
c_i	The ith bit of a codeword
d	Distance between constellation points
$\mathbb{E}\{\cdot\}$	Expectation operator
$\mathcal{E}_s$	Energy per symbol
$\mathbb{F}_s$	Finite field s
γ_s	SNR per symbol
$\Im(\cdot)$	Imaginary part of a complex number
Λ	Half distance between adjacent constellation points in M-QAM
λ	Average number of immediate neighbors of a constellation point

$\oplus$	Addition over finite field $\mathbb{F}_2$
M	Modulation-level of Node A
N	Modulation-level of Node B
m	$\log_2(M)$
n	$\log_2(N)$
μ_i	Total number of bit differences
N_0	Single-sided noise power spectral density
Ω	Signal constellation set
ω_c	Carrier frequency
$\mathbb{P}[\cdot]$	Probability of an event
P_b	Bit-error probability
P_s	Symbol-error probability
$Q(\cdot)$	Complementary cumulative distribution function of the Normal distribution
$\Re(\cdot)$	Real part of a complex number
$\bar{\rho}_i$	Average number of bit errors per constellation point
$\bar{\xi}_i$	Total average number of bit errors per constellation point
σ_i^2	Variance of a Gaussian random variable
T_s	Modulation interval
τ_i	Number of immediate neighbors of a constellation point
W^j	The jth message
$\mathcal{Y}_i$	Demodulated signal set
Z_i	Circularly symmetric complex Gaussian random variable

Chapter 1

Introduction

In 1893, Nikola Tesla presented to the world a wireless experiment that has tremendously influenced modern society. His vision was to use his invention for transmitting information, as mentioned in his article [1], where he described broadcasting as a method for "*enlightening the masses*". A few years later, in 1901, Guglielmo Marconi made headlines worldwide, when he sent the letter "s" wirelessly across the Atlantic from Poldhu, England to St. John's, Newfoundland, Canada [2, 3], and a new era was born.

Wireless communication has advanced dramatically since the early days of Tesla and Marconi; WiFi[1], Bluetooth[2], and WiMAX[3], are just a few of the recent advancements in this field. Nowadays, new wireless networks such as wireless body area networks (WBANs), vehicular ad-hoc networks (VANETs), and wireless sensor networks (WSNs) are being developed to benefit public health, driver safety, and the environment. Today, wireless

[1]Wireless Fidelity (WiFi) is a brand name for certified products that comply with the IEEE 802.11 standard.

[2]Bluetooth is a standard for short-range radio communication, currently adopted by the IEEE 802.15.1 standard.

[3]Worldwide Interoperability for Microwave Access (WiMAX) is the commercial name of products that comply with the IEEE 802.16 standard.

communication is one of the fastest growing sectors in the industry, mainly driven by the growth of the Internet. As of June 2009, the number of cellular subscribers has globally reached to 4.3 billion [4], and the number is still growing.

The increasing demand on wireless technology has made the spectrum a scarce resource. Research in millimeter-wave, cognitive radio, and ultra-wideband communications, are some of the latest trends to utilize what still can be used of the spectrum. Tight power regulations have further increased the challenges on already-constrained wireless networks.

Recently, network coding has attracted considerable research attention since the seminal paper by Ahlswede *et al.* [5], which showed the advantage of coding over routing. Despite the simple idea behind network coding, it can increase throughput [6], minimize the energy per bit [7], and significantly reduce delays in networks [8]. The promises of network coding have moved it from academia to industry. Lately, Avalanche [9], a project by Microsoft, has been one of the first to implement network coding in peer-to-peer file distribution systems.

In digital communication, there are various modulation schemes, e.g., M-PSK, M-QAM, etc., each with its own capabilities and limitations. Selecting a suitable modulation scheme for transmission is based on the channel condition and desired performance. Bandwidth efficiency, bit-error rate (BER) performance, and hardware implementation are some of the general trade-offs made during modulation scheme selection. Additionally, the importance of choosing a particular modulation scheme appears in coded modulation, where the coding gain can be further increased when an appropriate modulation schemes is used [10]. Therefore, modulation scheme selection is a vital step in the design of any communication system.

The deployment of network coding in wireless networks has received a lot of research attention, mainly due to the capability of network coding to improve throughput and save

energy. Yet, the broadcast phase in wireless network coding is challenged by the diverse rate requirements of receivers. This is especially notable in fading environments, where link capacities are time-varying. A simple way to determine the broadcasting rate is the minimum rate policy, which is based on transmitting at the lowest rate required by receivers. By this conservative approach, an acceptable BER can be maintained. However, the cost is an insufficient utilization of the available channel capacity. Therefore, a poor channel is a bottleneck of networks that employ such a policy. Cover [11] was the first to study the capacity of the broadcast channel; he showed that using a time-sharing approach the lower bound of the maximum achievable transmission rate can be achieved. In this approach, portions of time were allocated to transmission at different rates. Moreover, the information-theoretic study in [11] showed that a more efficient way of broadcasting information than time-sharing can be achieved by superposition coding. In [12], a practical way of implementing this, called embedded modulation, was presented, and is also known in the literature as hierarchical and multi-resolution modulation. In contrast to the proposed scheme, embedded modulation can only partially satisfy receivers in terms of BER for a given signal-to-noise ratio (SNR). This is due to the non-uniform spacing of constellation points in embedded modulation. In [13], a multilevel coding scheme was devised; in this scheme error-correction codes are used for protecting several bit streams, and then coded bits are assigned to constellation points. However, the proposed scheme is based on mapping bits to constellation points based on the availability of side information at end-nodes.

In [14], nested coding was introduced and the benefits of combining network coding with channel coding were presented. In [15], nested coding was used to enable diverse modulation requirements. Yet, the cost is a naturally coded constellation, resulting in a

higher BER than the proposed scheme which can maintain Gray code mapping.

1.1 Research Challenge and Motivation

A challenging problem in wireless network coding is to determine which modulation scheme to employ in the broadcast phase for receivers that have diverse modulation scheme requirements. For example, Node A may desire an 8-PSK modulation scheme on the broadcasted signal, while Node B may require a QPSK on the same signal. Such a scenario typically occurs when one receiver has a high channel capacity, while the other has a low one. Although rich literature can be found on wireless network coding, there has been little discussion about this practical issue [16, 17, 18, 19, 20].

The specific aim of this thesis can be summarized by the following statement:
Code design for the broadcast phase in wireless network coding to satisfy receivers that have diverse modulation requirements on a shared broadcasted signal.

Our main contributions in this thesis are twofold. First, we design codes for the broadcast phase in wireless network coding to deal with the diverse modulation problem. Second, we analyze the performance of the proposed codes.

1.2 Thesis Outline

The remainder of the thesis is organized as follows. In Chapter 2, an overview of network coding, followed by a brief review of digital modulation schemes, is presented. In Chapter 3, the system model is described. In Chapter 4, a coding scheme to deal with the diverse modulation problem is proposed; codes for several pairs of modulation schemes

are presented, and their performance is analyzed in Chapter 5. In Chapter 6, simulation results are presented to evaluate the performance of the proposed scheme and validate the accuracy of our analytical model. Finally, Chapter 7 concludes the thesis with a summary and future work.

Chapter 2

Preliminary

2.1 Network Coding

Ahlswede *et al.* [5] broadly defined network coding as "coding at a node in a network". A more specific definition by [21] was "coding at a node in a network with error-free links". This clarification was made to separate network coding from channel coding schemes, in which redundancy is added to achieve reliable communication.

In conventional routing, nodes store and forward data they receive, whereas in network coding nodes are allowed to encode data (Figure 2.1). When nodes are given this capability, a sender can attain the theoretical maximum rate for communicating common information to receivers. This maximum rate is known as the multicasting capacity of a network.

The butterfly network in Figure 2.2 can be used to illustrate how network coding can improve throughput. In this example Node S wishes to send bits b_1 and b_2 to both t_1 and t_2. Here, all links are assumed to have a unit capacity (1 bit/sec); if conventional routing is used whereby nodes store and forward data, then Node C would be capable only of sending

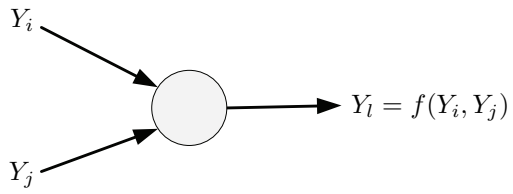

Figure 2.1: Network coding at an intermediate node.

either b_1 or b_2 (Figure 2.3). Accordingly, both of the destination nodes would share the central link CD, resulting in an information flow of 3/2 ($bits/sec$) to each of these nodes. However, the maximum information flow predicted by the min-cut/max-flow theorem for this network is 2 ($bits/sec$). Hence, conventional routing is generally suboptimal in terms of bandwidth efficiency.

Alternatively, in network coding, Node C can combine both bits by addition over finite field $\mathbb{F}_2$[1], ($b_1 \oplus b_2$), and send this combination to both destination nodes (Figure 2.4). Node t_1 can extract b_2 from this combination by $b_2 = b_1 \oplus (b_1 \oplus b_2)$. In a similar way node t_2 can extract b_1 by $b_1 = b_2 \oplus (b_1 \oplus b_2)$. Using this approach, the maximum information flow to both destination nodes can be achieved.

2.1.1 Linear Coding

Generally, the encoding process can be described as follows: let $\{W^1, W^2, \ldots, W^n\}$ be a set of messages generated by a source or multiple sources within a network. Moreover, let $\{g_1, g_2, \ldots, g_n\}$ be a set of coefficients chosen from finite field $\mathbb{F}_{2^s}$. In linear network coding, the encoded message at an intermediate node can be written as

[1]Addition over finite field $\mathbb{F}_2$ is bitwise exclusive-or, denoted as $\oplus$.

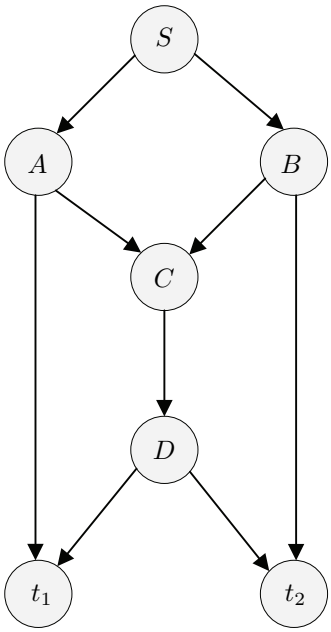

Figure 2.2: Butterfly network.

$$X = \sum_{i=1}^{n} g_i W^i. \tag{2.1}$$

Here, $\boldsymbol{g} = (g_1, g_2, \ldots, g_n)$ is called the encoding vector, and X is called the information vector. Once destination nodes receive several encoded messages, $X_1, X_2, \ldots, X_k$, with their associate encoding vectors, $\boldsymbol{g}_1, \boldsymbol{g}_2, \ldots, \boldsymbol{g}_k$, they can decode these messages by solving the following system of equations, where the unknowns are W^i:

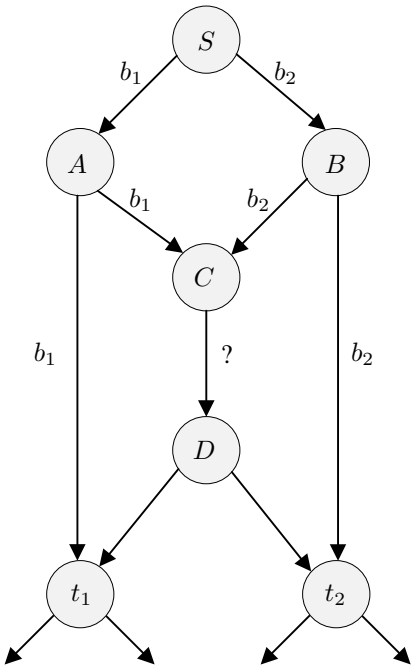

Figure 2.3: Routing in butterfly network.

$$
\begin{aligned}
X_1 &= \sum_{i=1}^{n} g_i^1 W^i \\
X_2 &= \sum_{i=1}^{n} g_i^2 W^i \\
&\vdots \\
X_k &= \sum_{i=1}^{n} g_i^k W^i
\end{aligned}
\tag{2.2}
$$

However, to decode the received messages, *i.e.,* to solve the system of equations, destination nodes must receive at least n linear independent combinations of the original messages.

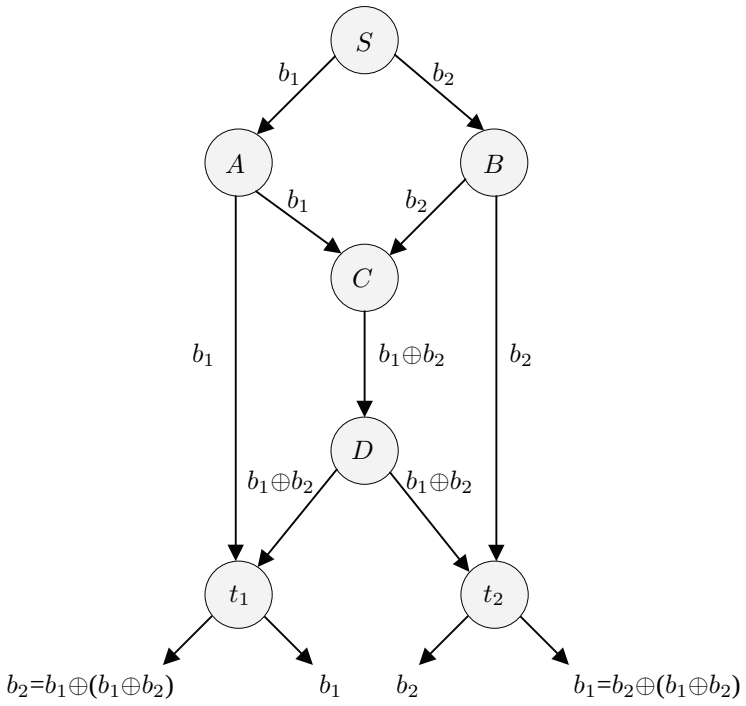

Figure 2.4: Network coding in butterfly network.

2.1.2 Wireless Network Coding

Wireless network coding is an extension of network coding to wireless environments; it can be illustrated by first showing how information is exchanged in a two-way relay channel (Figure 2.5) by traditional relaying and then, by how network coding can be used to perform this exact exchange with fewer transmissions:

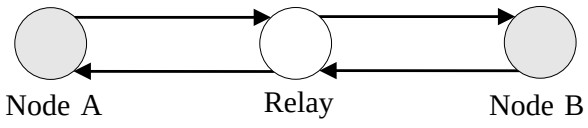

Figure 2.5: Two-way relay channel.

Traditional Relaying

Consider the basic building block of wireless network coding, depicted in Figure 2.5, where Node A and Node B communicate via a relay in a half-duplex mode, *i.e.*, nodes cannot transmit and receive data at the same time. In traditional relaying, Node A sends a message, W_a, to the relay, which relays it to Node B, and similarly Node B sends a message, W_b, to the relay, which in turn, relays it to Node A. Hence, exchanging a pair of messages requires four transmissions (Figure 2.6).

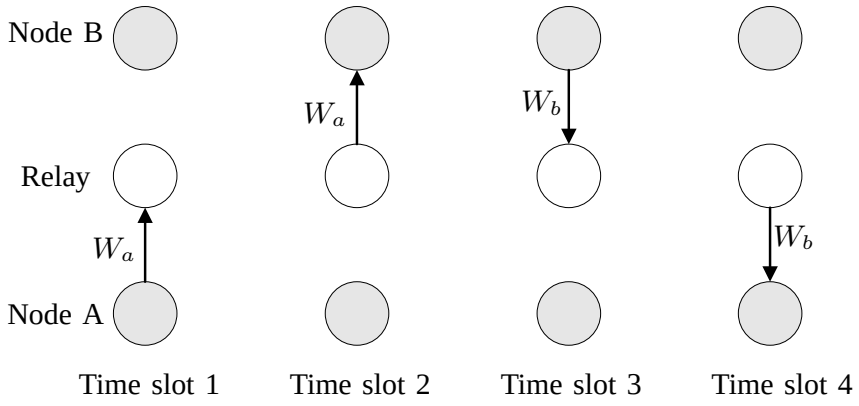

Figure 2.6: Traditional relaying.

Wireless Network Coding

Here, we show how network coding reduces the number of transmissions. A simple way of implementing network coding in the two-way relay channel is to allow the relay to combine messages by addition over finite field $\mathbb{F}_2$ [22],[16].

In this scheme, Node A and Node B send their messages sequentially to the relay; the relay then combines both messages by performing the $\oplus$ operation and broadcasts a new message, W_c=$W_a \oplus W_b$, to both nodes (Figure 2.7). Node A can extract Node B's message by simply performing the $\oplus$ operation on the received message with the messages it sent, W_b=$W_c \oplus W_a$. Similarly, Node B can extract Node A's message in the same way, W_a=$W_c \oplus W_b$. With this approach, network coding reduces the number of transmissions needed to exchange a pair of messages to three.

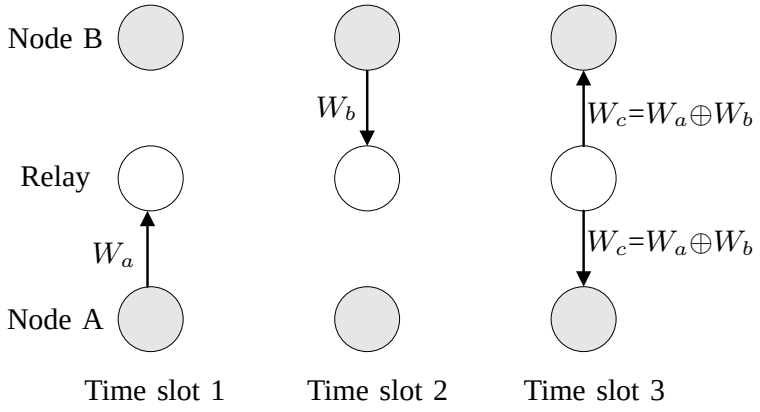

Figure 2.7: Wireless network coding.

2.2 Digital Modulation

Digital modulation provides the means of conveying information across a channel; it is generally defined as mapping a sequence of symbols to a set of waveforms. Many modulation schemes can be found in the literature; some of the most well-know are phase-shift keying (PSK), quadrature amplitude modulation (QAM), and frequency-shift keying (FSK).

Digital modulation schemes can be classified as either linear or non-linear, depending on which parameter of a sinusoidal carries information. In linear modulation schemes, such as PSK and QAM, information is encoded in the phase/amplitude, whereas in non-linear modulation schemes, such as FSK, information is encoded in the frequency.

Linear modulation schemes are more spectral efficient than non-linear schemes. However, non-linear schemes have the advantage of being less susceptible to fading and interference [23]. Depending on the desired performance and channel condition, one may prefer one modulation scheme over the other.

2.2.1 M-ary Phase-Shift Keying (M-PSK)

M-PSK is one of the most widely used modulation schemes; it has the advantage of being simple to generate [24], and it has been adopted by various standards, for example, CDMA2000 [25], DVB-S2 [26], and IEEE 802.16 [27].

In M-PSK, during each modulation interval, T_s, a modulator maps a block of m-bits to a carrier phase. A special form of PSK is binary phase-shift keying (BPSK), where the phase of the carrier is shifted by 0 or π radians, depending on whether a 0 or 1 was sent. The general waveform expression of M-PSK is

$$s(t) = Ap(t)\cos(\omega_c t + \theta_i), \qquad 0 \leq t \leq T_s, \tag{2.3}$$

$$\theta_i = \frac{2\pi i}{M}, \qquad i = 0, 1, \ldots, M-1, \tag{2.4}$$

where A is the signal's amplitude, $p(t)$ is the pulse shape, and ω_c is the frequency of the carrier. Common M-PSK constellations and their decision boundaries are shown in Figure 2.8.

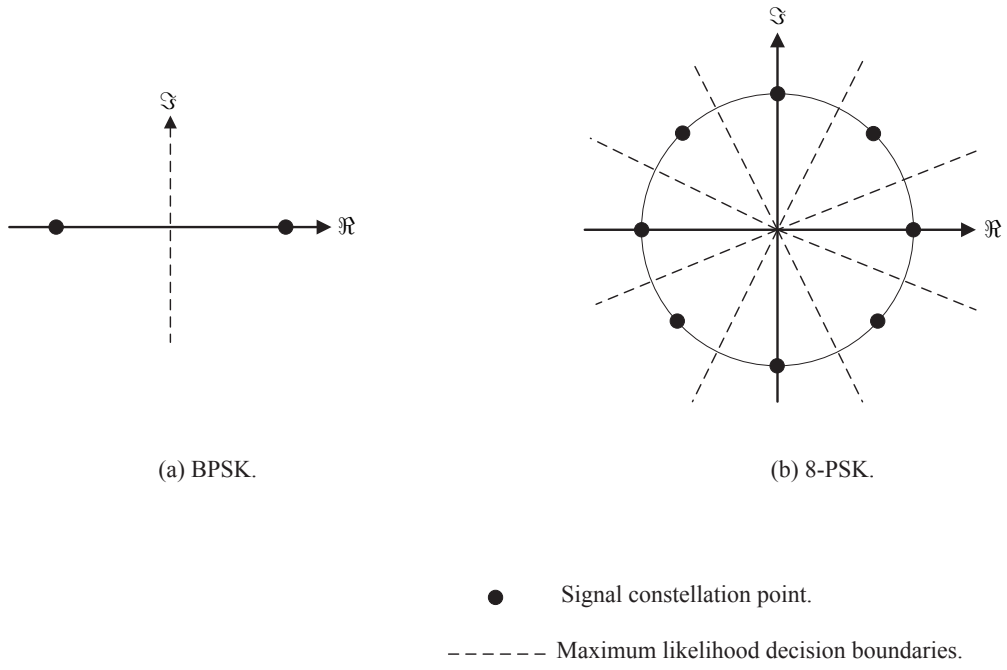

Figure 2.8: M-PSK constellation diagrams.

2.2.2 M-ary Quadrature Amplitude Modulation (M-QAM)

In 1960, R. C. Cahn extended PSK to a scheme that has a blend of digital amplitude and phase modulation, and was subsequently called M-QAM [28]. Today, M-QAM is becoming an attractive modulation scheme to meet the fast-growing demands on higher data rates, mainly due to its power and spectral efficiency. Recent standards such as DVB-T2 [29], IEEE 802.15.3 [30], and IEEE 802.20 [31] employ M-QAM for data transmission. In M-QAM the data is conveyed by changing the amplitude and phase of a carrier. The M-QAM waveform can be expressed as follows

$$s(t) = A_i p(t) \cos(\omega_c t + \varphi_i), \qquad 0 \leq t \leq T_s, \tag{2.5}$$

where $A_i = \sqrt{u_i + v_i}$ and $\varphi_i = \tan^{-1}(v_i/u_i)$. For square M-QAM constellations,(e.g., 16-QAM, 64-QAM, 256-QAM), u_i and v_i independently take values form the finite set

$$\Phi = \{ \ (2i - \sqrt{M} + 1) \mid \ i = 0, 1, \ldots, \sqrt{M} - 1 \ \}.$$

Figure 2.9 shows some common M-QAM constellations diagrams and their decision boundaries.

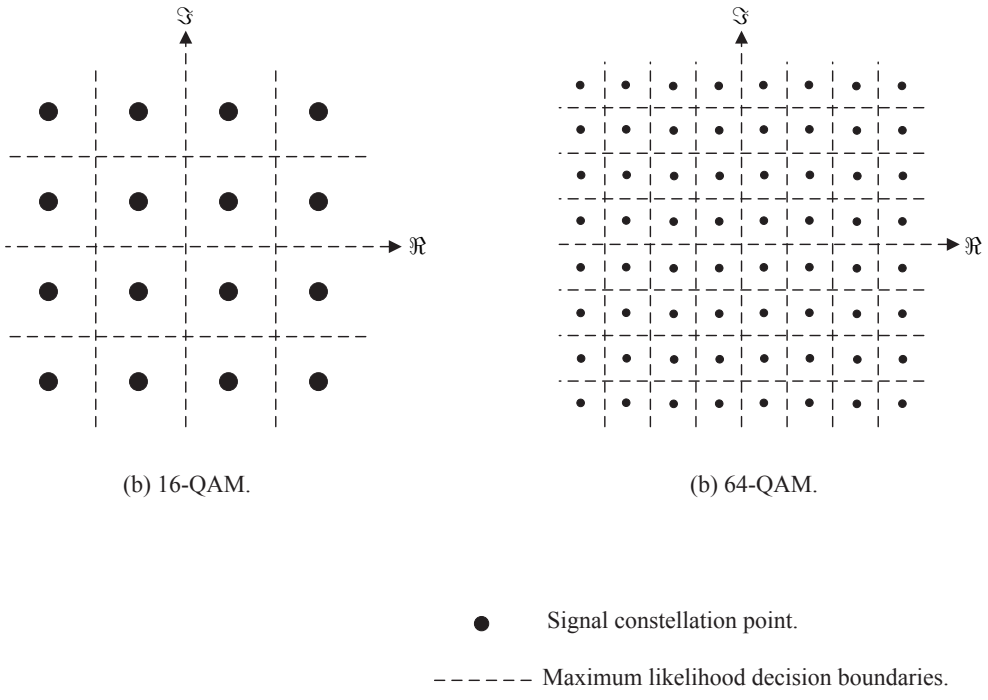

(b) 16-QAM. (b) 64-QAM.

Figure 2.9: M-QAM constellation diagrams.

Chapter 3

System Model

Consider a wireless communication scenario, where two nodes exchange a pair of messages. We assume there is no direct connection between end-nodes. Accordingly, a relay is used to assist the communication (Figure 2.5). All Nodes within the network operate in a half-duplex mode. We also assume that all messages generated by sources are equally probable. We consider 2^m-PSK and square 2^m-QAM modulation schemes, where a modulator maps a block of m-coded bits to a complex channel symbol

$$f : C_i \rightarrow X \in \Omega, \tag{3.1}$$

where $C_i \in \{0, 1\}^m$ is the output of the encoder, described in Chapter 4, and Ω is the signal constellation set

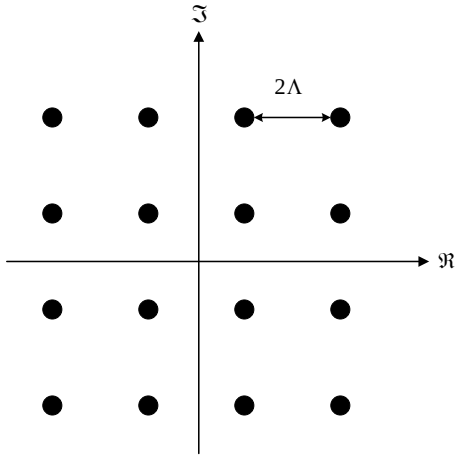

Figure 3.1: Spacing between adjacent constellation points of a 16-QAM.

$$\Omega = \left\{ \begin{array}{ll} \sqrt{\mathcal{E}_s}\cos\left(j\frac{2\pi\ell}{2^m}\right) + j\sqrt{\mathcal{E}_s}\sin\left(j\frac{2\pi\ell}{2^m}\right) & \mid \ell = 0,\ldots,2^m-1, \qquad \text{for } 2^m\text{-PSK} \\ \Lambda(2i-\sqrt{2^m}+1) + j\Lambda(2k-\sqrt{2^m}+1) & \mid i,k = 0,1,\ldots,\sqrt{2^m}-1, \text{ for } 2^m\text{-QAM} \end{array} \right\},$$

where $\mathcal{E}_s$ is the energy per symbol, 2Λ is the spacing between adjacent constellation points (Figure 3.1), and $j{=}\sqrt{-1}$. We focus on the broadcast phase, *i.e.,* the third time slot in Figure 2.7, where a relay broadcasts a signal to two receivers through an additive white Gaussian noise (AWGN) channel. Therefore, the input and output are given by

$$Y_1 = X + Z_1, \tag{3.2}$$

$$Y_2 = X + Z_2, \tag{3.3}$$

where X is constrained to an average power $\mathbb{E}\{|X|^2\} \leq P$, Y_1 and Y_2 are the outputs at Nodes A and B, respectively, and Z_1 and Z_2 are circularly symmetric[1] complex Gaussian random variables, with variances of σ_1^2 and σ_2^2, respectively. The demodulated signal at end-nodes takes a value from the finite set $\mathcal{Y}_i = \{0, 1, \ldots, 2^m - 1\},\ i \in \{1, 2\}$.

In the broadcast phase, we assume that the relay has perfect knowledge of the channel condition, and accordingly selects the most suitable modulation scheme for end-nodes. Additionally, we assume that the modulation-level required by Node A is higher than that of Node B, *i.e.*, Node A requires an M-ary modulation scheme, whereas Node B requires an N-ary modulation scheme, where M>N.

[1]A complex Gaussian random variable $Z = X + jY$ is circularly symmetric if Z and $Ze^{j\theta}$ have the same distribution for any θ.

Chapter 4

Proposed Modulation-Level Coding Scheme

In this chapter, we present the coding scheme proposed to deal with the diverse modulation requirements of receivers. Suppose that Node A requires a 2^m-ary modulation scheme and Node B requires a 2^n-ary modulation scheme, where $m > n$. Let $\boldsymbol{\alpha}$ and $\boldsymbol{\beta}$ denote the binary sequences of Nodes A and B at the relay, respectively:

$$\boldsymbol{\alpha} = (a_1^1, a_1^2, \ldots, a_1^n, \ldots, a_l^1, a_l^2, \ldots, a_l^n), \qquad a_l^j \in \{0, 1\},$$

$$\boldsymbol{\beta} = (b_1^1, b_1^2, \ldots, b_1^m, \ldots, b_l^1, b_l^2, \ldots, b_l^m), \qquad b_l^j \in \{0, 1\},$$

where a_l^j is the jth bit in a n-tuple, and a similar notation is used to describe the elements in $\boldsymbol{\beta}$.

Encoder: The encoder at the relay maps inputs from Nodes A and B to form a codeword C_i, selected from a codebook $\mathbf{C} = (C_1, C_2, \ldots, C_M)$, $C_i = (c_1, c_2, \ldots, c_m)$, where each

$c_i \in \{0, 1\}$;

$$\psi : \{0, 1, \ldots, 2^n - 1\} \times \{0, 1, \ldots, 2^m - 1\} \rightarrow \mathbf{C}. \tag{4.1}$$

Decoder: The decoders at Nodes A and B use side information to decode the received message

$$\phi_1 : \{0, 1, \ldots, 2^n - 1\} \times \mathcal{Y}_1 \rightarrow \{0, 1, \ldots, 2^m - 1\}, \tag{4.2}$$

$$\phi_2 : \{0, 1, \ldots, 2^m - 1\} \times \mathcal{Y}_2 \rightarrow \{0, 1, \ldots, 2^n - 1\}, \tag{4.3}$$

where ϕ_1 and ϕ_2 are the decoders at Nodes A and B, respectively. The encoding and decoding rules are based on trellis diagrams, which are presented shortly.

The aim of the proposed coding scheme is to: (i) satisfy nodes with unlike modulation-level requirements; (ii) maximize the Euclidean distance between adjacent constellation points. These objectives can be achieved by partitioning a constellation of size 2^m into 2^{m-n} subsets, such that the Euclidean distance between adjacent constellation points within each subset is maximized. Figure 4.2 illustrates a QPSK constellation partitioned into two BPSK subsets and corresponding trellis diagrams used for mapping input bits to codewords, and vice versa. Various combinations of modulation schemes and associated trellis diagrams are shown in Figures 4.6–4.8; further extensions of M-PSK diagrams can be found in Appendix A.

Using the proposed scheme, the relay can broadcast a codeword, C_i, to both nodes using the high modulation-level, *i.e.,* the 2^m-ary modulation scheme. Upon receiving a codeword, Nodes A and B use their side information and codebook $\mathbf{C}$ to decode the received message. Figure 4.1 summarizes the communication process of the proposed scheme.

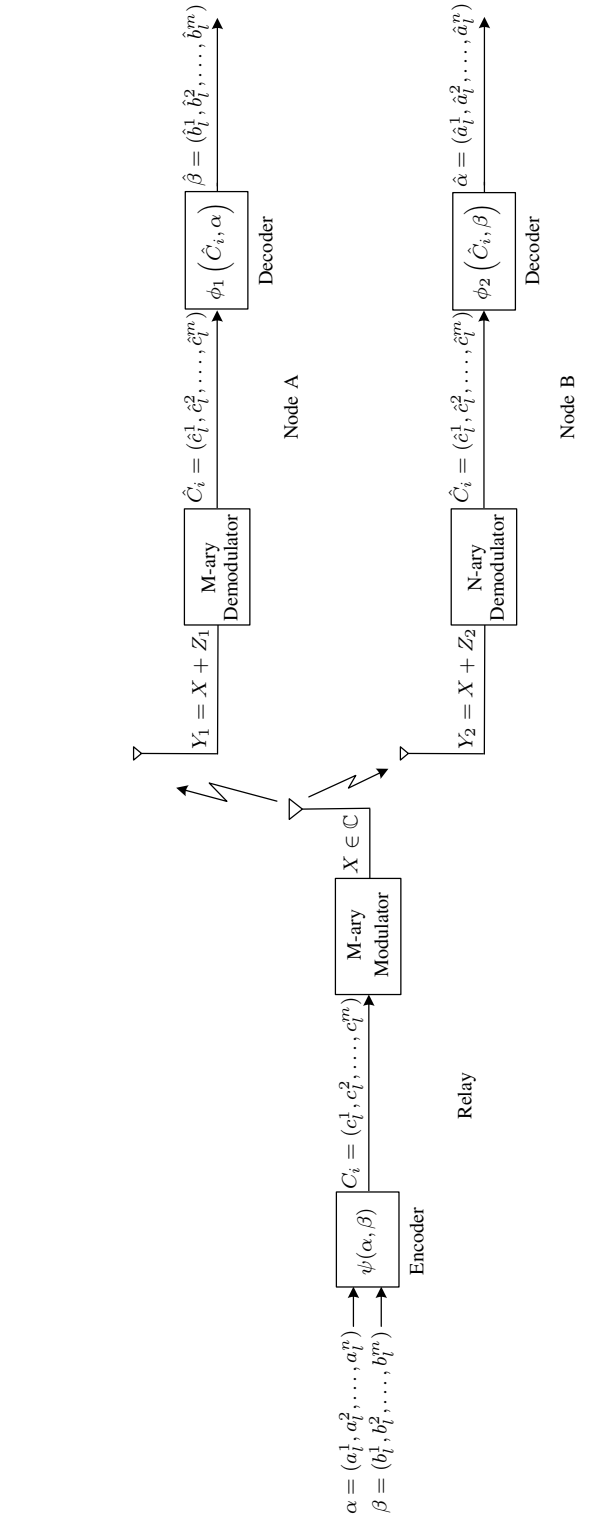

Figure 4.1: Communication process using the proposed scheme.

We use a simple example to illustrate the operation of the proposed coding scheme. Suppose Node A's channel can support QPSK *(2 bits/sec/Hz)*, whereas Node B's channel can support only BPSK *(1 bits/sec/Hz)*. Moreover, for simplicity, suppose that Node A sends the following bit, a_l^1=1, and Node B sends the bits $b_l^1 b_l^2$=10. In this coding scheme, the trellis diagram in Figure 4.2(c), is used for encoding the input bits from Nodes A and B to form a codeword. In this particular example, the bits of the codeword are $c_l^1 c_l^2$=01. Subsequently, the relay broadcasts these coded bits using the high modulation-level, *i.e.*, QPSK.

Detection and decoding of the broadcasted signal at end-nodes are different. Node A uses a QPSK constellation diagram for detection (Figure 4.3), which comprises four decision regions. Next, Node A decodes the received message by knowledge it sent a_l^1=1 and the received coded bits $c_l^1 c_l^2$=01, which together correspond in the trellis diagram in Figure 4.2(c), to $b_l^1 b_l^2$=10.

On the other hand, Node B perceives the received QPSK signal as a BPSK signal, since it knows the bits it sent $b_l^1 b_l^2$, and also knows that only one bit from Node A is encoded in the broadcasted symbol. Referring to Figure 4.2(c), the number of possible received codewords for Node B is just two, (*i.e.*, it can be either $c_l^1 c_l^2$=10 if a_l^1=0 or $c_l^1 c_l^2$=01 if a_l^1=1). Hence, there are just two decision regions, R_0 and R_1; if the observed signal falls in R_0, the decision made is that 01 was sent, and 10 if it falls in R_1 (Figure 4.4).

Once Node B has demodulated the received signal, it decodes $c_l^1 c_l^2$=01 using its own side information $b_l^1 b_l^2$=10. These values together correspond in the trellis diagram in Figure 4.2(c), to a_l^1=1.

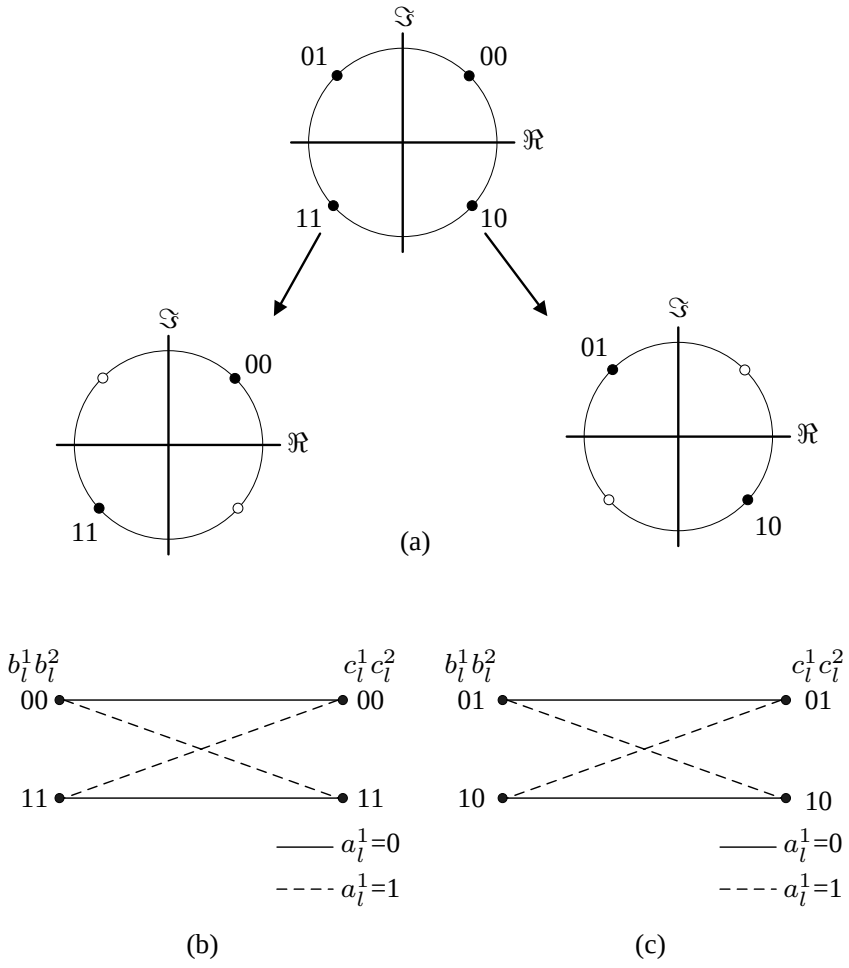

Figure 4.2: (a) Partitioning a QPSK constellation into two BPSK subsets, (b)-(c) Two-state trellis diagrams for encoding and decoding, for m=2, n=1, where $\{a_l^i\}$ and $\{b_l^i\}$ are inputs bits from Nodes A and B, respectively; and $\{c_l^i\}$ are bits of output codeword.

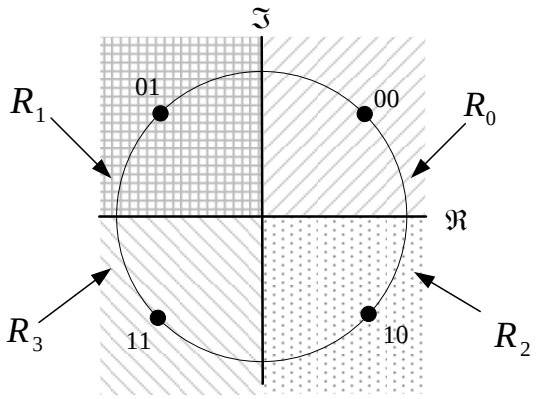

Figure 4.3: Decision regions for Node A, QPSK.

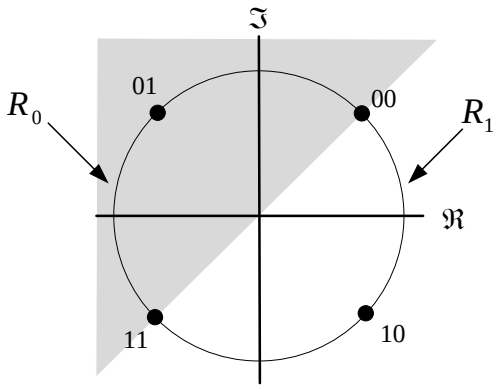

Figure 4.4: Decision regions for a QPSK perceived as a BPSK, when $b_l^1 b_l^2 = 10$ or $b_l^1 b_l^2 = 01$, for Node B.

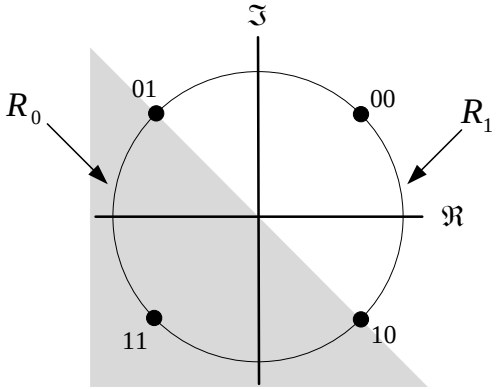

Figure 4.5: Decision regions for a QPSK perceived as a BPSK, when $b_l^1 b_l^2 = 00$ or $b_l^1 b_l^2 = 11$, for Node B.

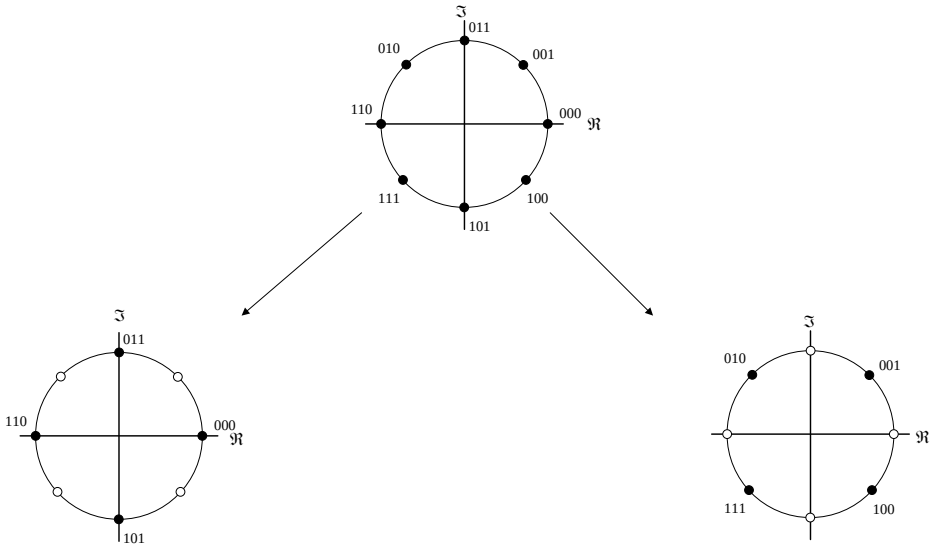

(a)

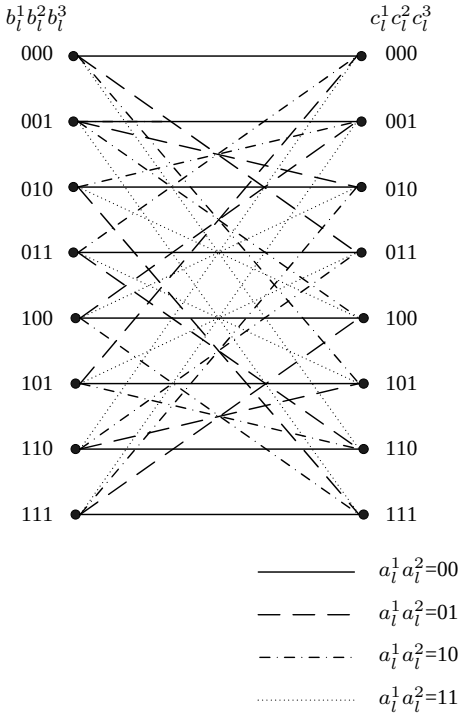

(b)

Figure 4.6: (a)8-PSK/QPSK constellation partitioning (b)Eight-state trellis diagram for encoding and decoding, for m=3, n=2, where $\{a_l^i\}$ and $\{b_l^i\}$ are inputs bits from Nodes A and B, respectively; and $\{c_l^i\}$ are bits of output codeword.

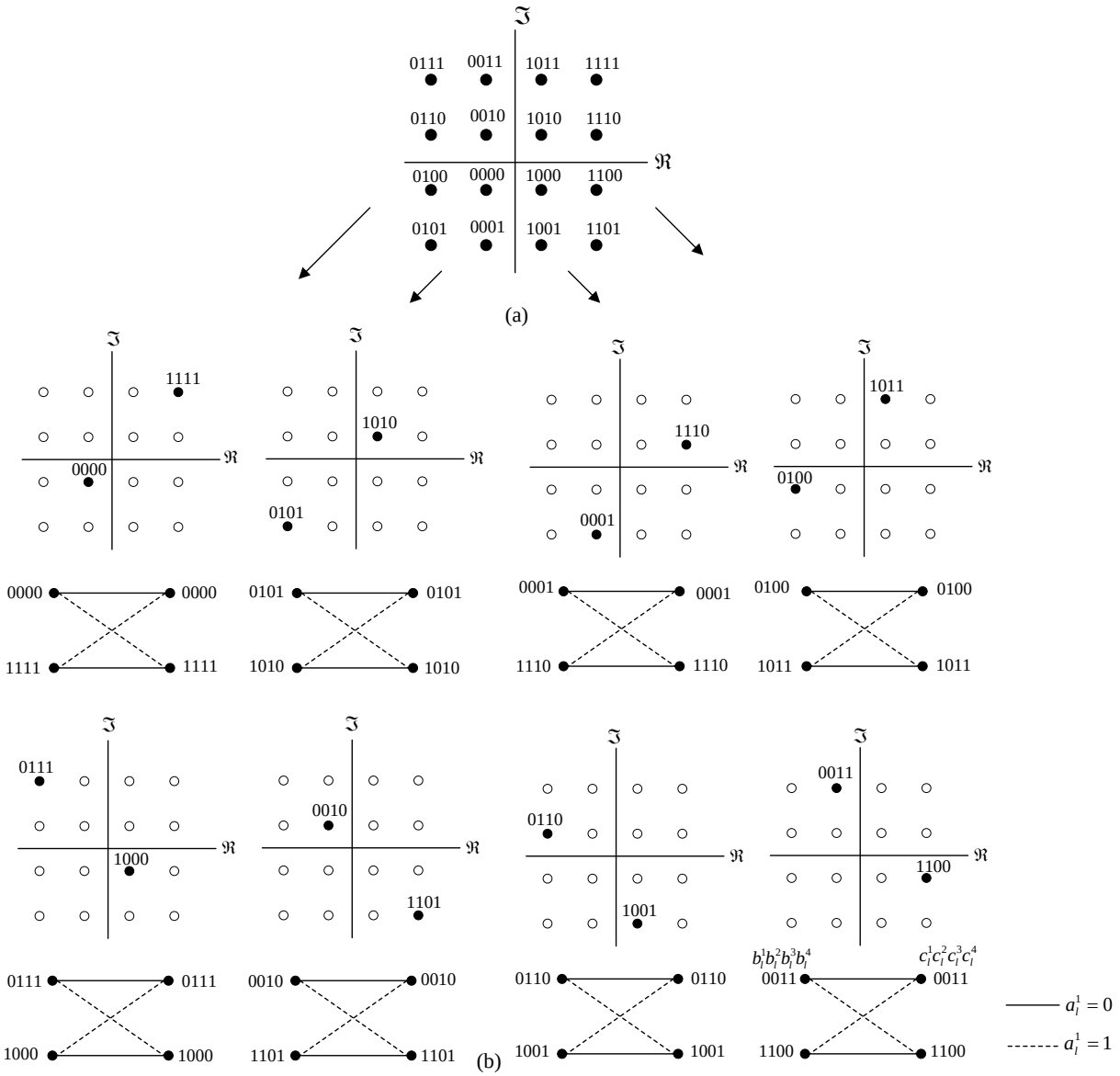

Figure 4.7: (a) Partitioning 16-QAM constellation into Semi-BPSK subsets, (b)Two-state trellis diagrams for encoding and decoding, for m=4, n=1, where $\{a_l^i\}$ and $\{b_l^i\}$ are inputs bits from Nodes A and B, respectively; and $\{c_l^i\}$ are bits of output codeword.

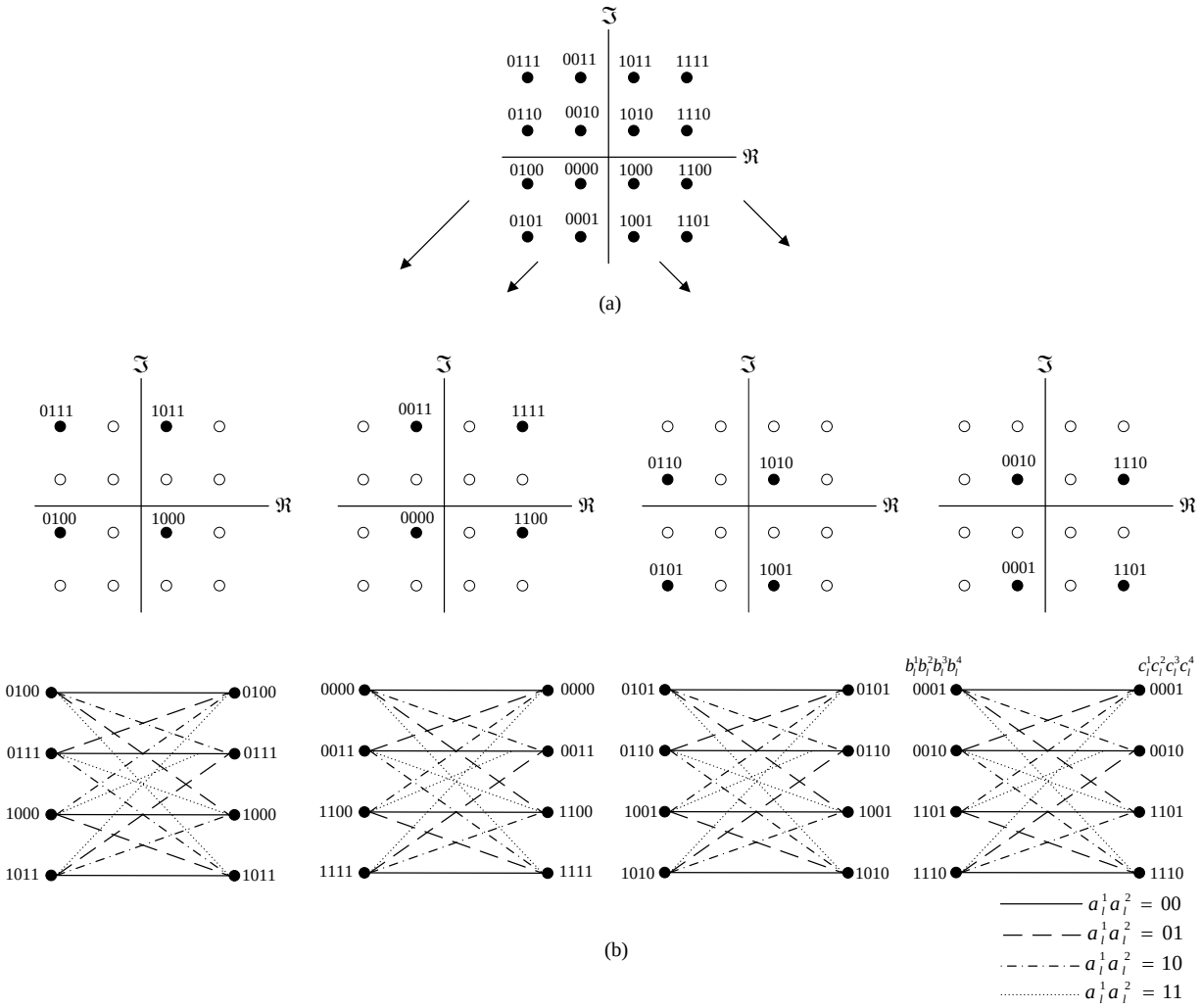

Figure 4.8: (a) Partitioning 16-QAM constellation into Semi-QPSK subsets, (b) Four-state trellis diagrams for encoding and decoding, for m=4, n=2, where $\{a_l^i\}$ and $\{b_l^i\}$ are inputs bits from Nodes A and B, respectively; and $\{c_l^i\}$ are bits of output codeword.

Chapter 5

Performance Analysis

In this chapter, the performance of the proposed scheme is analyzed in terms of bit-error probability[1], which is then validated by simulation in Chapter 6. The number of possible received symbols for the same broadcasted signal at end-nodes is different. For Node A, from (4.1), there are 2^m possible symbols since there are m unknown bits encoded for it in each broadcasted symbol. On the other hand, from (4.1), there are n unknown bits encoded for Node B in each broadcasted symbol, which results in 2^n possible symbols. Therefore, by the proposed coding scheme, Node B can perceive a 2^m-ary constellation as a 2^n-ary.

5.1 Node A with 2^m-PSK and Node B with 2^n-PSK

For Node A, there are 2^m possible received symbols . Accordingly, for Gray-coded constellations[2] and using the nearest neighborhood approximation, the bit-error probability can

[1]The terms "bit-error probability" and "bit-error rate" are used interchangeably throughout the thesis.
[2]Adjacent constellation symbols in a Gray-coded constellation differ in only one bit.

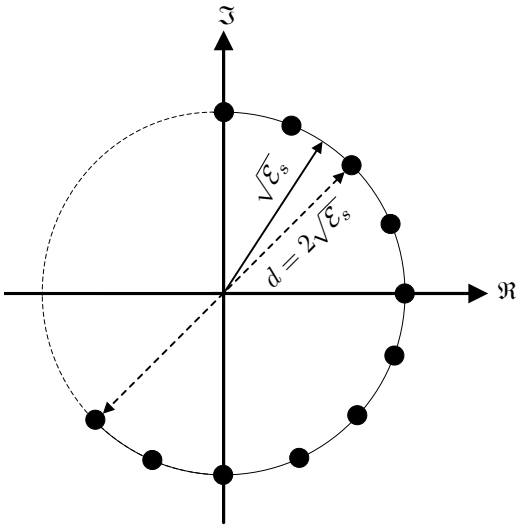

Figure 5.1: Distance between a pair of antipodal signals in M-PSK constellation.

be approximated by the well-known formula [32],

$$P_b \approx \frac{2}{m} Q\left(\sqrt{2\gamma_s}\ \sin\left(\frac{\pi}{2^m}\right)\right), \quad m > 1, \tag{5.1}$$

where γ_s denotes the SNR per symbol[3] and $Q(x) \triangleq \frac{1}{\sqrt{2\pi}} \int_x^\infty e^{-z^2/2}\, dz$.

When $n = 1$ (*i.e.*, BPSK), the distance, d, between a pair of antipodal signals is the diameter of the M-PSK constellation, $d = 2\sqrt{\mathcal{E}_s}$ (Figure 5.1). Consequently, the bit-error probability for Node B can be calculated by

$$\begin{aligned} P_b &= Q\left(\frac{d}{2\sigma}\right) \\ &= Q\left(\sqrt{2\gamma_s}\right) \qquad , \quad n = 1 \end{aligned} \tag{5.2}$$

[3] The SNR per symbol is defined as $\gamma_s \triangleq \dfrac{\mathcal{E}_s}{N_0}$, where N_0 is single-sided noise power spectral density in *(watts/Hz)*.

and well approximated by [32],

$$P_b \approx \frac{2}{n} Q\left(\sqrt{2\gamma_s}\ \sin\left(\frac{\pi}{2^n}\right)\right), \quad n > 1. \tag{5.3}$$

5.2 Node A with 16-QAM and Node B with BPSK

The definition of BPSK requires BPSK signals to have equal energies and a phase difference of π (*radians*) between constellation points. However, as shown in Figure 5.2, this definition can only be partially fulfilled by the proposed scheme. Therefore, we will call this proposed modulation scheme Semi-BPSK. The performance of Semi-BPSK compared to BPSK in terms of BER is shown in Figure 5.5.

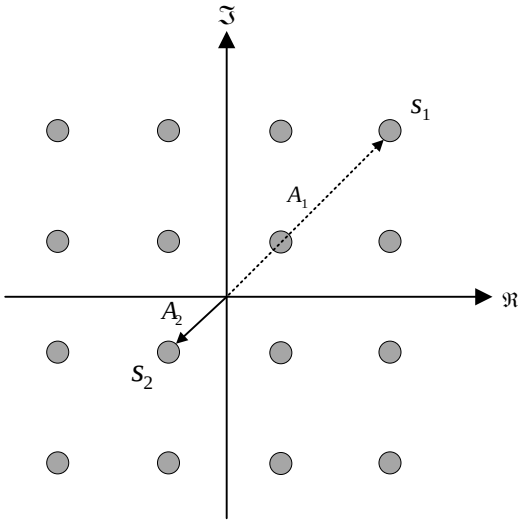

Figure 5.2: Semi-BPSK in 16-QAM constellation.

The nearest neighbor approximation can be used to calculate the symbol-error probability for an M-QAM scheme, which is given by

$$P_s \approx \lambda Q\left(\frac{d_a}{2\sigma}\right) = \lambda Q\left(\frac{\Lambda}{\sigma}\right), \tag{5.4}$$

where the average number of immediate neighbors of a constellation point is

$$\lambda = \frac{4(\sqrt{M}-2)^2 + 12(\sqrt{M}-2) + 8}{M}. \tag{5.5}$$

In M-QAM, the spacing between adjacent constellation points is $d_a = 2\Lambda$ (Figure 5.3), and the average energy of an M-QAM constellation can be calculated by [33],

$$\mathcal{E}_s = \frac{4\Lambda^2 \sum_{i=0}^{\sqrt{M}/2-1}(2i+1)^2}{\sqrt{M}}. \tag{5.6}$$

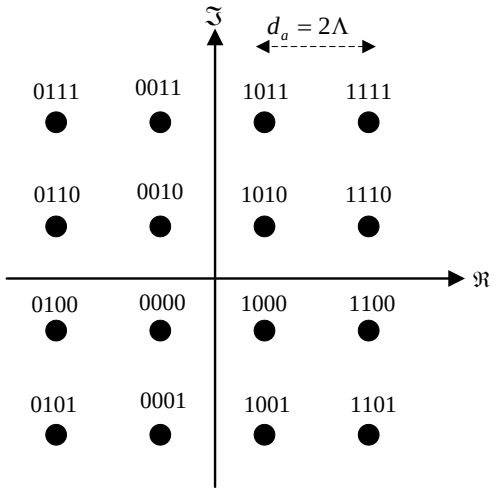

Figure 5.3: Distance between adjacent constellation points for 16-QAM.

From (5.5) and (5.6), the values of λ and Λ for a 16-QAM constellation are 3 and $\sqrt{\frac{\mathcal{E}_s}{10}}$,

respectively. Substituting these values in (5.4) yields

$$P_s \approx 3Q\left(\sqrt{\frac{\gamma_s}{5}}\right). \tag{5.7}$$

Since the constellation in Figure 5.3 is Gray-coded, the bit-error probability for Node A can be approximated by

$$P_b \approx \frac{P_s}{4} \approx \frac{3}{4}Q\left(\sqrt{\frac{\gamma_s}{5}}\right). \tag{5.8}$$

On the other hand, Node B perceives the 16-QAM constellation as a Semi-BPSK by the proposed coding scheme. Accordingly, the bit-error probability is given by

$$P_b = Q\left(\frac{d_b}{2\sigma}\right), \tag{5.9}$$

where d_b is the distance between a pair of Semi-BPSK constellation points (Figure 5.4), which is $d_b = 4\sqrt{2}\Lambda$. From (5.6), the values of Λ for 16-QAM constellation is $\sqrt{\frac{\mathcal{E}_s}{10}}$; therefore, $d_b = 4\sqrt{\frac{\mathcal{E}_s}{5}}$; substituting the value of d_b in (5.9), we get the bit-error probability of Node B

$$P_b = Q\left(\sqrt{\frac{8\gamma_s}{5}}\right). \tag{5.10}$$

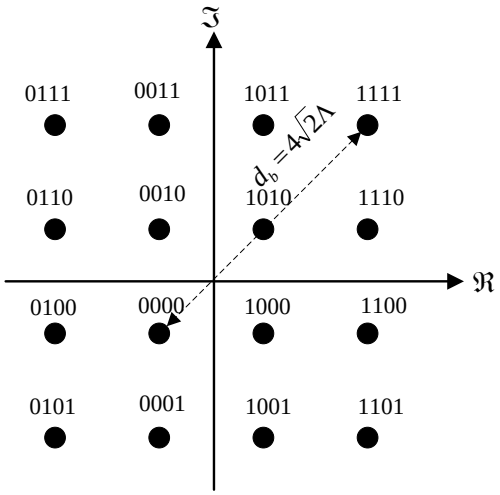

Figure 5.4: Distance between a pair of Semi-BPSK symbols in 16-QAM constellation.

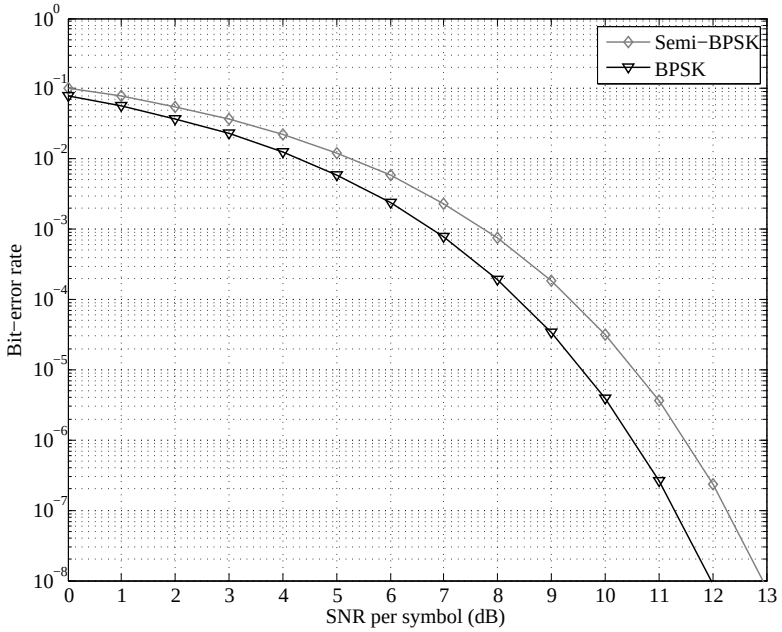

Figure 5.5: Comparison of bit-error rate performance versus SNR over AWGN channel for Semi-BPSK and BPSK.

5.3 Node A with 16-QAM and Node B with QPSK

The definition of QPSK requires QPSK signals to have equal amplitudes and phase shift differences of $\pi/2$ (*radians*). This definition can be only partially fulfilled by the proposed scheme (Figure 5.6). Hence, we will call this proposed modulation scheme Semi-QPSK. The comparison between QPSK and Semi-QPSK in terms of BER is shown in Figure 5.8.

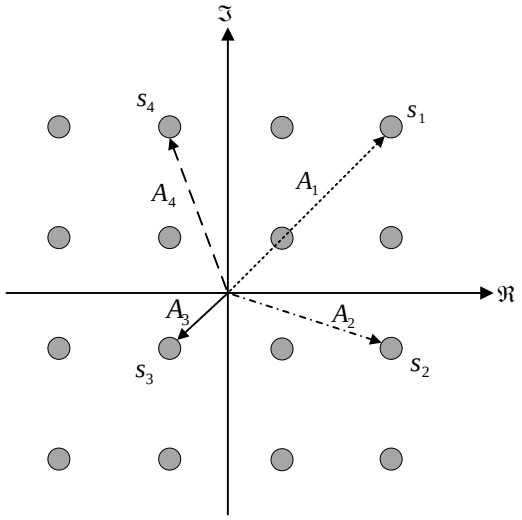

Figure 5.6: Semi-QPSK in 16-QAM constellation.

From (5.7), the symbol-error probability for Node A is

$$P_s \approx 3Q\left(\sqrt{\frac{\gamma_s}{5}}\right). \tag{5.11}$$

However, calculating the bit-error probability is nontrivial due to the various combinations of decoded codewords on constellation points. Figure B.1, in Appendix B, illustrates this idea; in this figure, decoded codewords are placed on the constellation points for various values of $a_l^1 a_l^2$. As shown, when $a_l^1 a_l^2 = 00$ or $a_l^1 a_l^2 = 11$ Gray-coded constellations are maintained by the proposed scheme and are not when $a_l^1 a_l^2 = 01$ or $a_l^1 a_l^2 = 10$.

The general expression to calculate the bit-error probability for Node A is

$$P_b \approx \sum_{i=1}^{4} \frac{3}{4} \mathbb{P}\left[\mathbf{x} = S_i\right] \bar{\xi}_i Q\left(\sqrt{\frac{\gamma_s}{5}}\right), \tag{5.12}$$

where $\bar{\xi}_i$ is the total average number of bit errors per constellation point and $\mathbf{S}$ is the sample space that contains all possible combination of bits from Node A in each codeword. For the 16-QAM/Semi-QPSK trellis diagrams in Figure 4.8(b), we have

$$\begin{aligned} \mathbf{S} &= \{S_1, S_2, S_3, S_4\} \\ &= \{00, 01, 10, 11\} \end{aligned}$$

and

$$\begin{aligned} \bar{\boldsymbol{\xi}} &= \left\{\bar{\xi}_1, \bar{\xi}_2, \bar{\xi}_3, \bar{\xi}_4\right\} \\ &= \left\{1, \frac{19}{12}, \frac{19}{12}, 1\right\}. \end{aligned}$$

Detailed calculations of $\bar{\xi}_i$ will be given in Appendix B. Substituting the values of $\bar{\boldsymbol{\xi}}$ to (5.12), and for equally likely symbols from Node A, *i.e.,*

$$\mathbb{P}\left[\mathbf{x} = S_1\right] = \mathbb{P}\left[\mathbf{x} = S_2\right] = \mathbb{P}\left[\mathbf{x} = S_3\right] = \mathbb{P}\left[\mathbf{x} = S_4\right] = \frac{1}{4},$$

we get the bit-error probability for Node A,

$$P_b \approx \frac{31}{32} Q\left(\sqrt{\frac{\gamma_s}{5}}\right). \tag{5.13}$$

On the other hand, Node B perceives the 16-QAM constellation as Semi-QPSK by the proposed coding scheme. Therefore, the bit-error probability is given by

$$P_b \approx Q\left(\frac{d_b}{2\sigma}\right), \tag{5.14}$$

where the distance between a pair of Semi-QPSK constellation points (Figure 5.7) is $d_b = 4\Lambda$. From (5.6), the values of Λ for 16-QAM constellation is $\sqrt{\frac{\mathcal{E}_s}{10}}$; therefore, $d_b = 4\sqrt{\frac{\mathcal{E}_s}{10}}$. Substituting this value in (5.14), we get the bit-error probability of Node B

$$P_b \approx Q\left(\sqrt{\frac{4}{5}\gamma_s}\right). \tag{5.15}$$

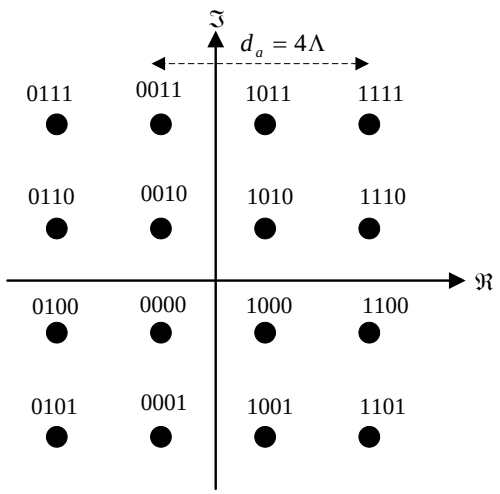

Figure 5.7: Distance between adjacent constellation points for Semi-QPSK in 16-QAM constellation.

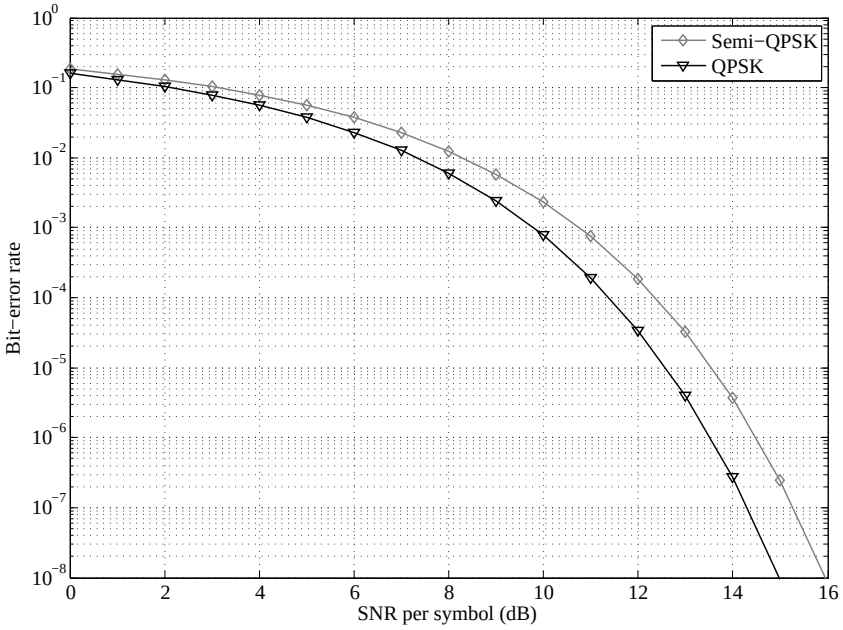

Figure 5.8: Comparison of bit-error rate performance versus SNR over AWGN channel for Semi-QPSK and QPSK.

5.4 An Upper Bound on P_b for Semi-BPSK

Proposition 5.4. *P_b of a Semi-BPSK in M-QAM constellation is upper-bounded by* $Q\left(\sqrt{\frac{3}{2}\gamma_s}\right)$.

Proof of Proposition 5.4. The bit-error probability for binary signaling is given by

$$P_b \;=\; Q\left(\frac{d}{2\sigma}\right), \tag{5.16}$$

and the distance between a pair of Semi-BPSK signals in M-QAM constellation is $d = \sqrt{2M}\Lambda$. For M-QAM constellations, Λ is given by [33],

$$\Lambda^2 = \frac{\mathcal{E}_s\sqrt{M}}{4\sum_{i=0}^{\sqrt{M}/2-1}(2i+1)^2}, \tag{5.17}$$

substituting the value of d in (5.16), and after some manipulation we get

$$P_b = Q\left(\sqrt{\frac{M^{3/2}}{4\left(4\sum_{i=0}^{\sqrt{M}/2-1} i^2 + 4\sum_{i=0}^{\sqrt{M}/2-1} i + \sum_{i=0}^{\sqrt{M}/2-1} 1\right)}\gamma_s}\right). \tag{5.18}$$

Using the following formulas

$$\sum_{i=1}^{n} i^2 = \frac{n(n+1)(2n+1)}{6}, \tag{5.19}$$

$$\sum_{i=1}^{n} i = \frac{n(n+1)}{2}, \tag{5.20}$$

$$\sum_{i=1}^{n} 1 = n, \tag{5.21}$$

(5.18) can be simplified to

$$P_b = Q\left(\sqrt{\frac{M^{3/2}}{\frac{2}{3}(M^{3/2}-\sqrt{M})}\gamma_s}\right). \tag{5.22}$$

Taking the limit, we get

$$\lim_{M\to\infty} Q\left(\sqrt{\frac{M^{3/2}}{\frac{2}{3}(M^{3/2}-\sqrt{M})}\gamma_s}\right) = Q\left(\sqrt{\frac{3}{2}\gamma_s}\right). \tag{5.23}$$

□

Figure 5.9 shows the performance of Semi-BPSK associated with several M-QAM constellations. As shown, the performance of Semi-BPSK changes with M. However, as the constellation size increases beyond M=64 the change in performance is relatively small and and is near the upper bound, e.g., the performance of Semi-BPSK in 64-QAM is almost the same as Semi-BPSK in 256-QAM.

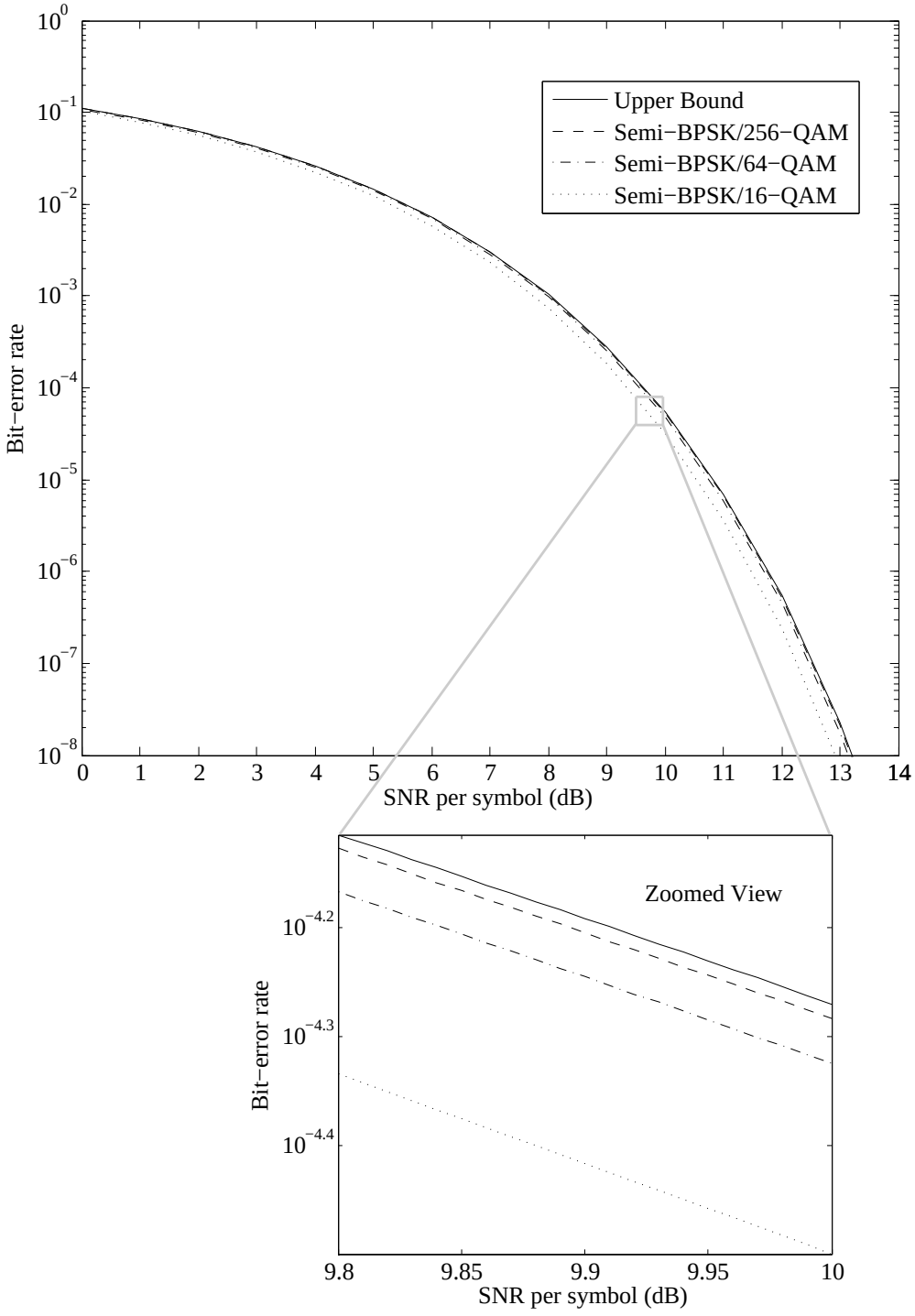

Figure 5.9: Bit-error rate performance of Semi-BPSK/M-QAM over AWGN channel.

Chapter 6

Simulation Results

In this chapter, we evaluate the performance of the proposed coding scheme and validate our analytical results via simulation. We consider the system setup described in Chapter 3. Additionally, the modulation requirement of Node A varies from QPSK to 16-QAM, while the modulation requirement of Node B varies from BPSK to 8-PSK. The trellis diagrams shown in Figures 4.2, 4.6-4.8, and A.2-A.5 are used for encoding and decoding. Moreover, the Gray-coded constellations in Figure 6.1 are used for mapping coded bits to signal points. In our simulations, maximum-likelihood (ML) receivers are used to select the the most probable sent signal, which is given by

$$\hat{X} = \underset{1 \le i \le M}{\arg\min} \left\| Y_1 - X_i \right\|^2, \quad \text{for Node A,} \tag{6.1}$$

$$\hat{X} = \underset{1 \le i \le N}{\arg\min} \left\| Y_2 - X_i \right\|^2, \quad \text{for Node B,} \tag{6.2}$$

where Y_i is the received signal, $\hat{X}$ is the estimation of the transmitted signal, and $X_i \in \Omega$.

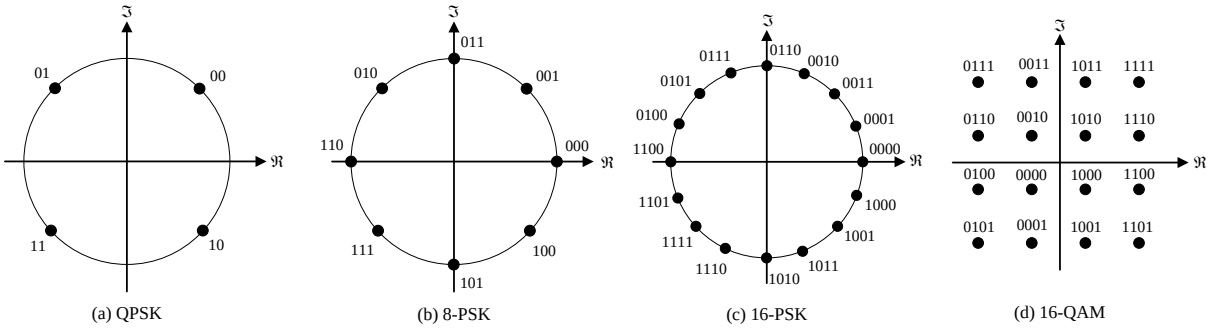

(a) QPSK (b) 8-PSK (c) 16-PSK (d) 16-QAM

Figure 6.1: Gray-coded constellations.

The simulation results in Figures 6.2-6.9 show performance of the proposed scheme across a wide range of SNRs. As shown, the BER performance takes the expected well-known waterfall curve since we considered a Gaussian channel, that is, at low SNRs the BER deceases gradually and falls dramatically at high SNRs.

Moreover, the comparisons in Figures 6.2-6.9 between the analytical and simulation results demonstrate the accuracy of our analytic model. However, there is a slight deviation between the simulation and analytical results. This is due to the nearest neighbor approximations used in our calculations.

Furthermore, the proposed scheme is compared with the scheme presented in [15]. As shown in Figure 6.10, the proposed scheme has an improved BER performance. This improvement comes from the careful coding design that maintains Gray code mapping. However, implementing the proposed scheme requires relays and end-nodes to have encoders and decoders.

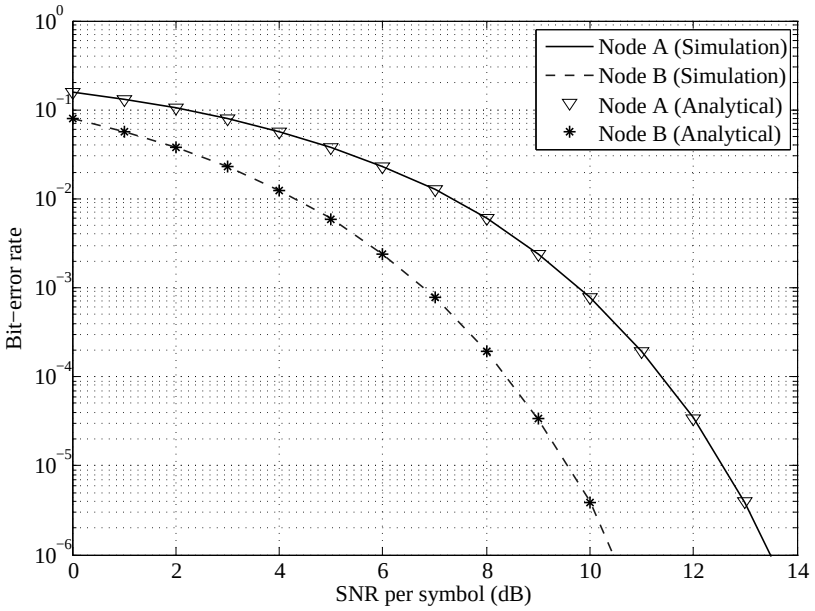

Figure 6.2: Bit-error rate performance over AWGN channel for Node A with QPSK and Node B with BPSK.

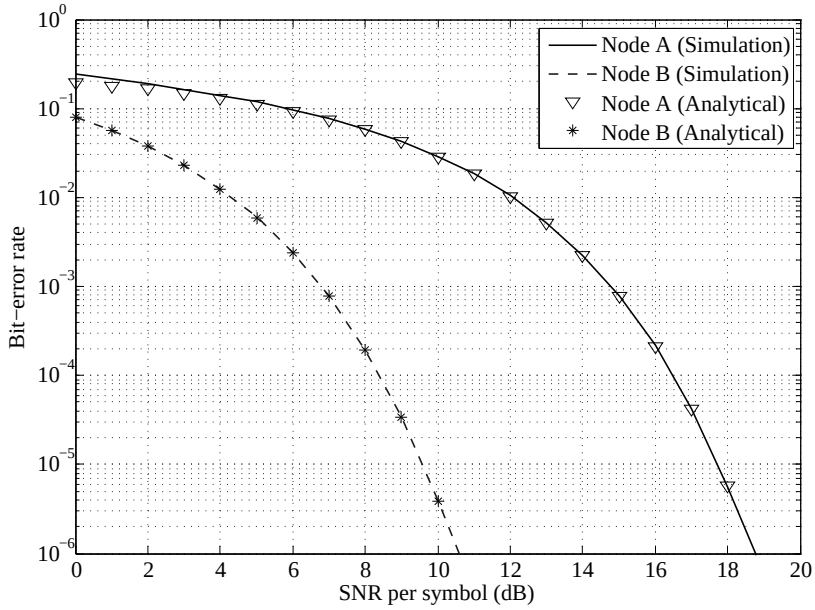

Figure 6.3: Bit-error rate performance over AWGN channel for Node A with 8-PSK and Node B with BPSK.

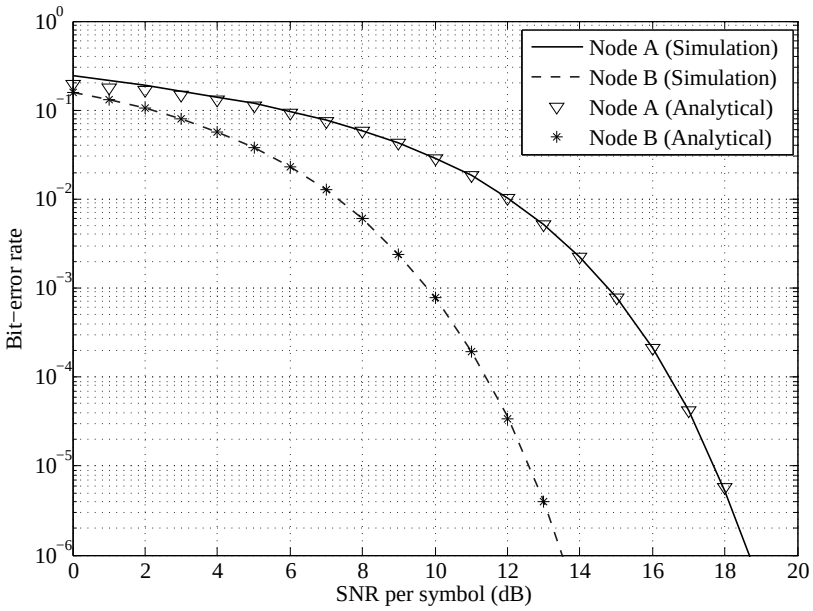

Figure 6.4: Bit-error rate performance over AWGN channel for Node A with 8-PSK and Node B with QPSK.

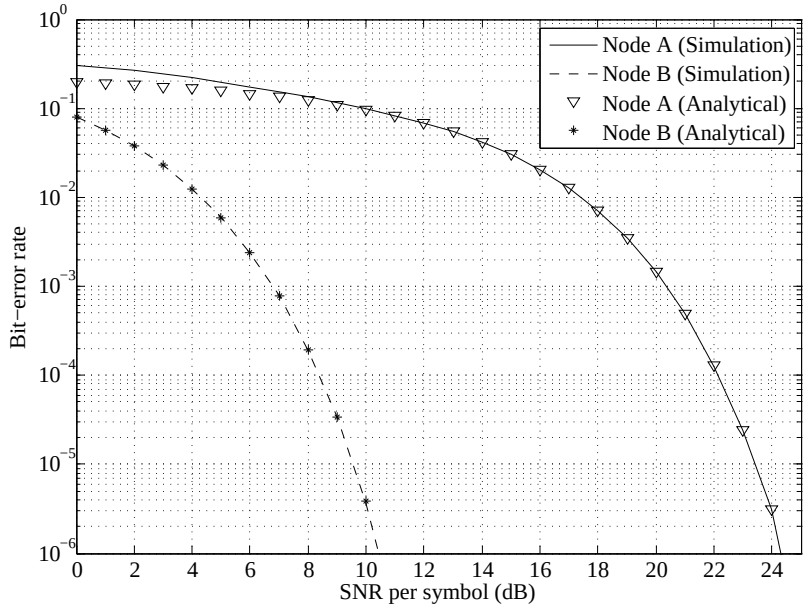

Figure 6.5: Bit-error rate performance over AWGN channel for Node A with 16-PSK and Node B with BPSK.

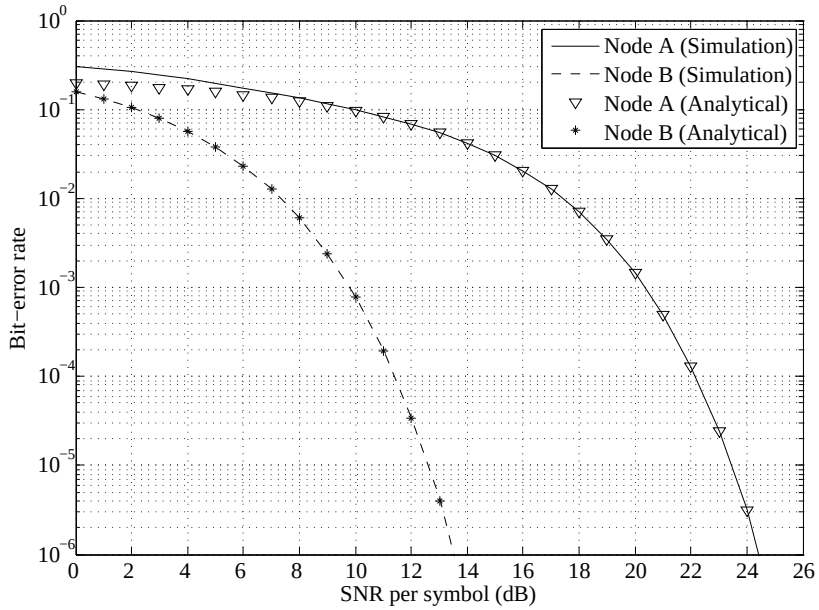

Figure 6.6: Bit-error rate performance over AWGN channel for Node A with 16-PSK and Node B with QPSK.

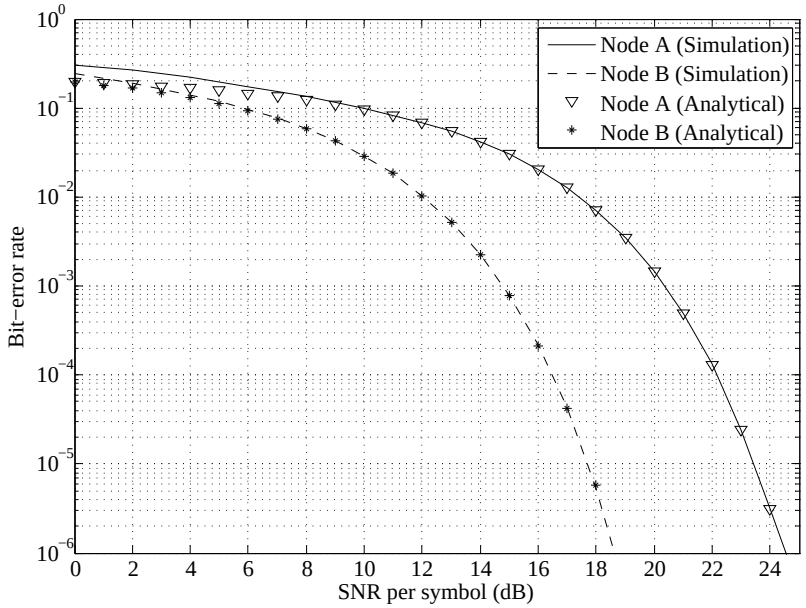

Figure 6.7: Bit-error rate performance over AWGN channel for Node A with 16-PSK and Node B with 8-PSK.

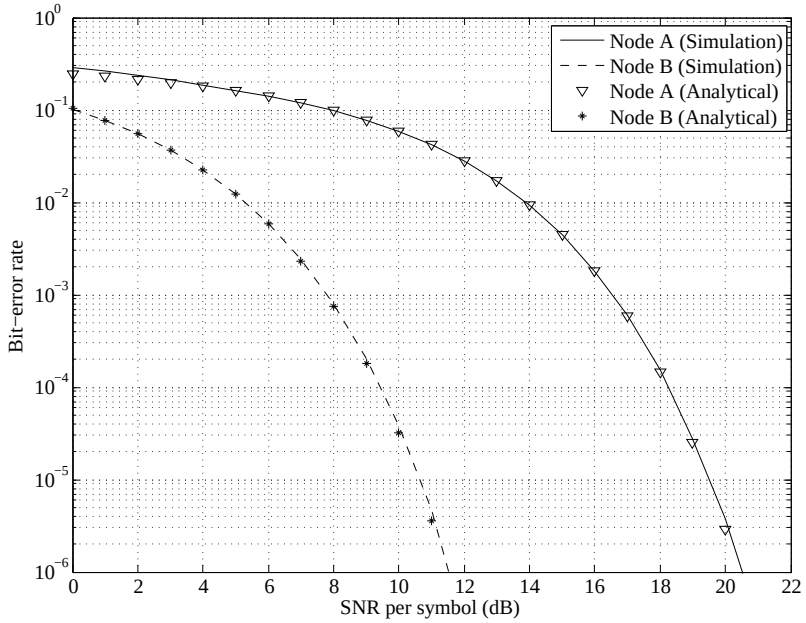

Figure 6.8: Bit-error rate performance over AWGN channel for Node A with 16-QAM and Node B with Semi-BPSK.

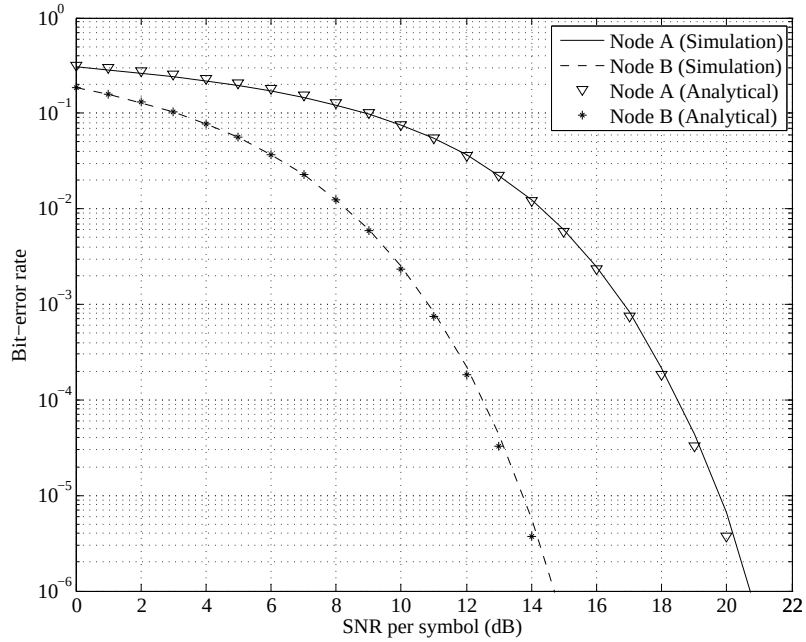

Figure 6.9: Bit-error rate performance over AWGN channel for Node A with 16-QAM and Node B with Semi-QPSK.

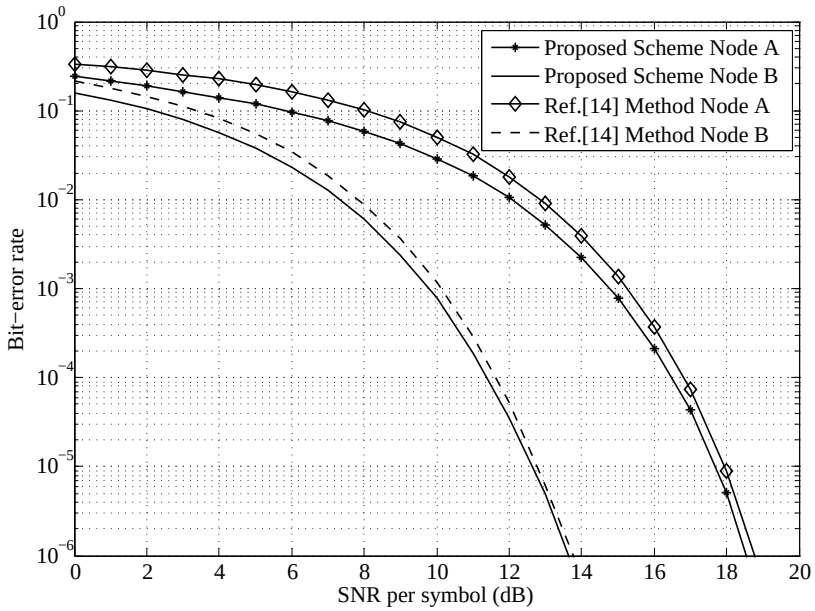

Figure 6.10: Comparison of bit-error rate performance versus SNR over AWGN channel for Node A with 8-PSK and Node B with QPSK.

Chapter 7

Summary and Future Work

7.1 Summary

In this thesis, a new coding scheme for wireless network coding is proposed to deal with the diverse modulation problem of receivers. The scheme is based on coding information such that a receiver with a high modulation-level requirement can decode more information from a broadcasted signal than a receiver with a low one. Several codes have been designed for various combinations of modulation schemes. The main advantage of the proposed scheme is that it enables wireless network-coded systems to efficiently utilize their available channel capacity.

Analytical studies have been carried out to quantify the performance of the proposed scheme. It is shown that individual modulation requirements can be fulfilled, when one receiver has an M-PSK requirement while the other has an N-PSK requirement, and can be partially fulfilled, with a very close performance, when one receiver has an M-QAM requirement while the other has an N-PSK requirement. Moreover, an upper bound on the

BER of Semi-BPSK has been found.

Extensive simulations have been conducted to demonstrate the performance of the proposed scheme and validate our analytic model. It is shown that the BER performance of the proposed scheme versus the SNR takes the well-known waterfall curve, which falls dramatically as the SNR increases. Comparisons between our analytical and simulation results demonstrate the accuracy of our analytic model. Additionally, the proposed scheme is compared with the scheme presented in [15]. Simulations show that the proposed scheme has an improved BER performance. This improvement comes from the careful coding design that maintains Gray code mapping.

7.2 Future Work

In this thesis, we have introduced a new coding scheme for wireless network coding aimed at solving the diverse modulation problem of receivers. However, there are still several issues that need to be further investigated:

First, the research work presented in this thesis focuses on designing codes for the two-way relay channel, where there are two end-nodes. Our work can be further extended to a more general network where there are multiple nodes communicating via a relay. The challenge of designing codes in this topology lies in the availability of side information at end-nodes and the multiple modulation scheme requirements.

Second, in this research we focused on the broadcast phase in wireless network coding. Our analytical results can be extended to include the uplink phase. Obviously, decoding errors in the uplink phase will have a high impact on the BER in the downlink phase, this interaction needs further investigation.

Finally, in our work we assumed that the relay has perfect knowledge of the channel condition, and accordingly selects the most suitable modulation scheme for receivers. However, in practice, knowledge of the channel condition is imperfect. In this situation, robust broadcasting can be achieved if the proposed scheme is jointly designed with error-correction codes.

APPENDICES

Appendix A

Trellis Diagrams

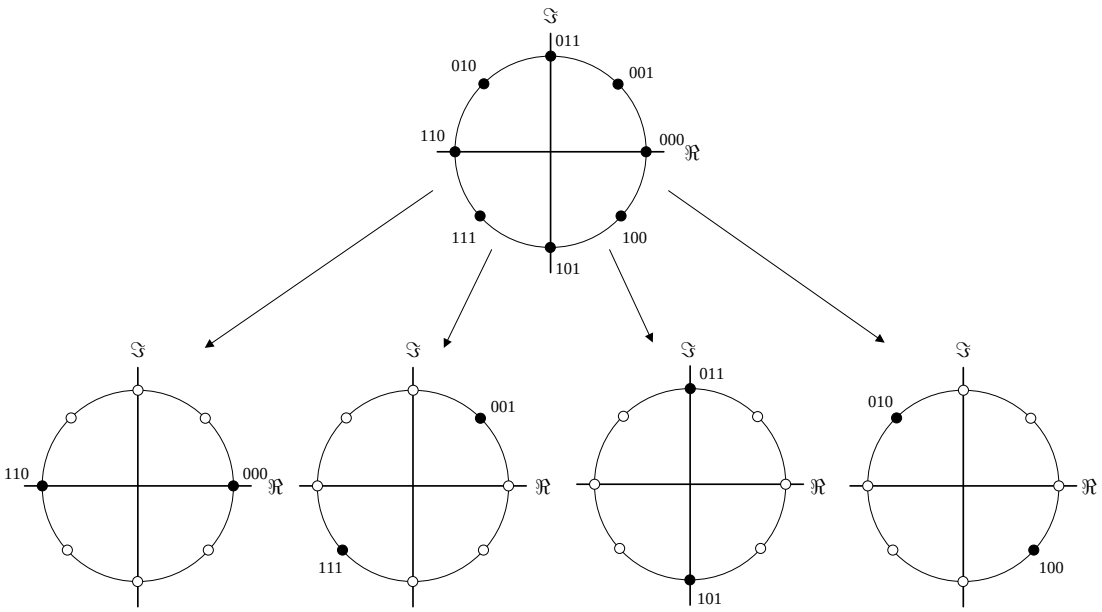

Figure A.1: 8-PSK/BPSK constellation partitioning.

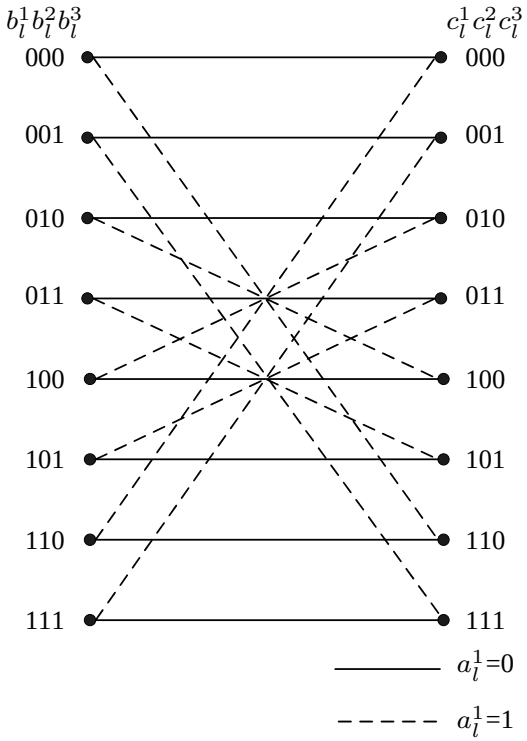

Figure A.2: 8-PSK/BPSK trellis diagram for encoding and decoding, m=3, n=1, where $\{a_l^i\}$ and $\{b_l^i\}$ are inputs bits from Nodes A and B, respectively; and $\{c_l^i\}$ are bits of output codeword.

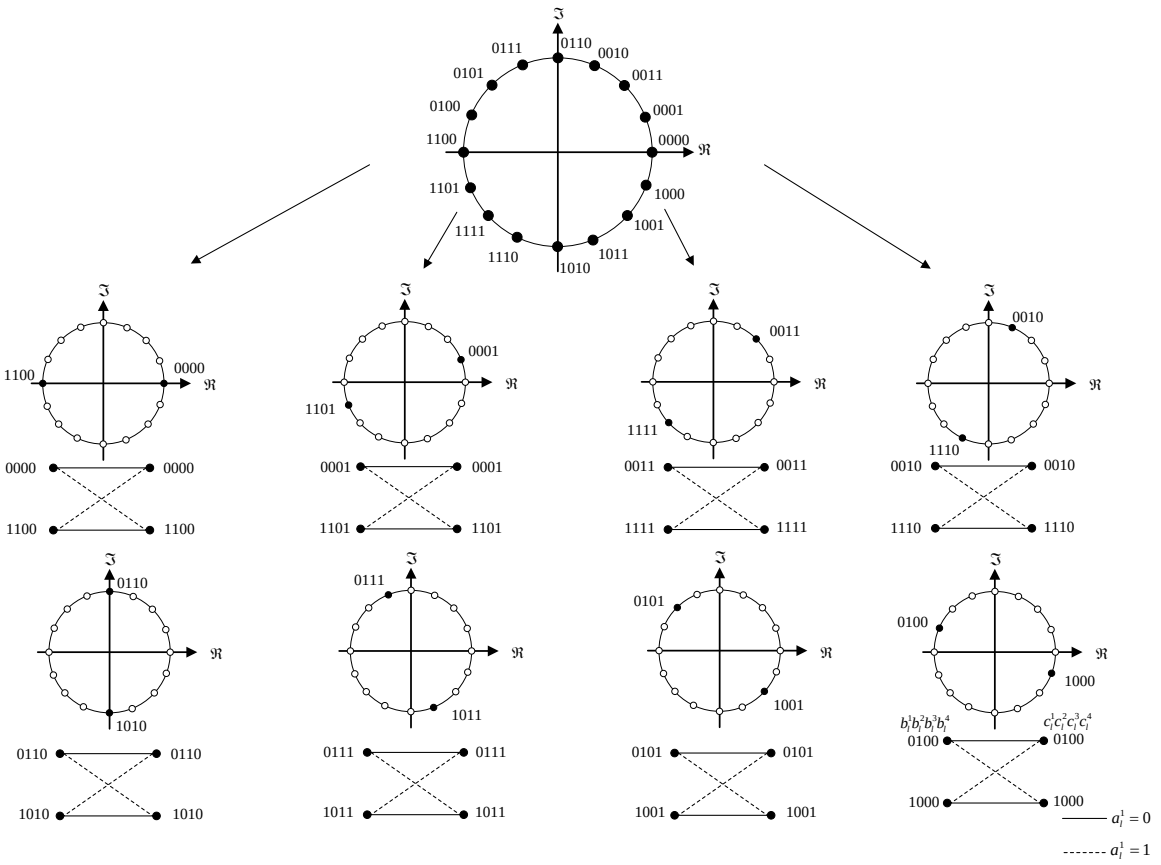

Figure A.3: 16-PSK/BPSK constellation partitioning and trellis diagrams for encoding and decoding, m=4, n=1, where $\{a_l^i\}$ and $\{b_l^i\}$ are inputs bits from Nodes A and B, respectively; and $\{c_l^i\}$ are bits of output codeword.

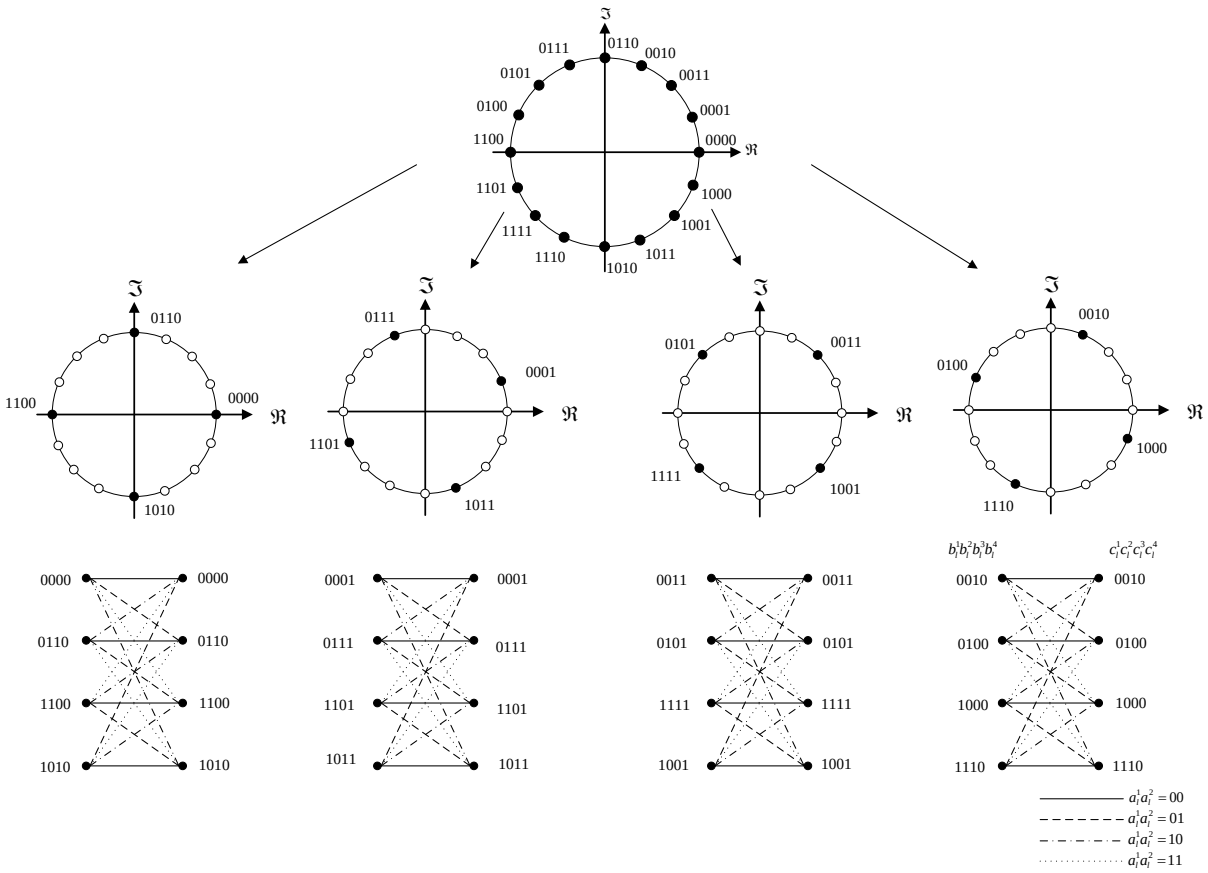

Figure A.4: 16-PSK/QPSK constellation partitioning and trellis diagrams for encoding and decoding, m=4, n=2, where $\{a_l^i\}$ and $\{b_l^i\}$ are inputs bits from Nodes A and B, respectively; and $\{c_l^i\}$ are bits of output codeword.

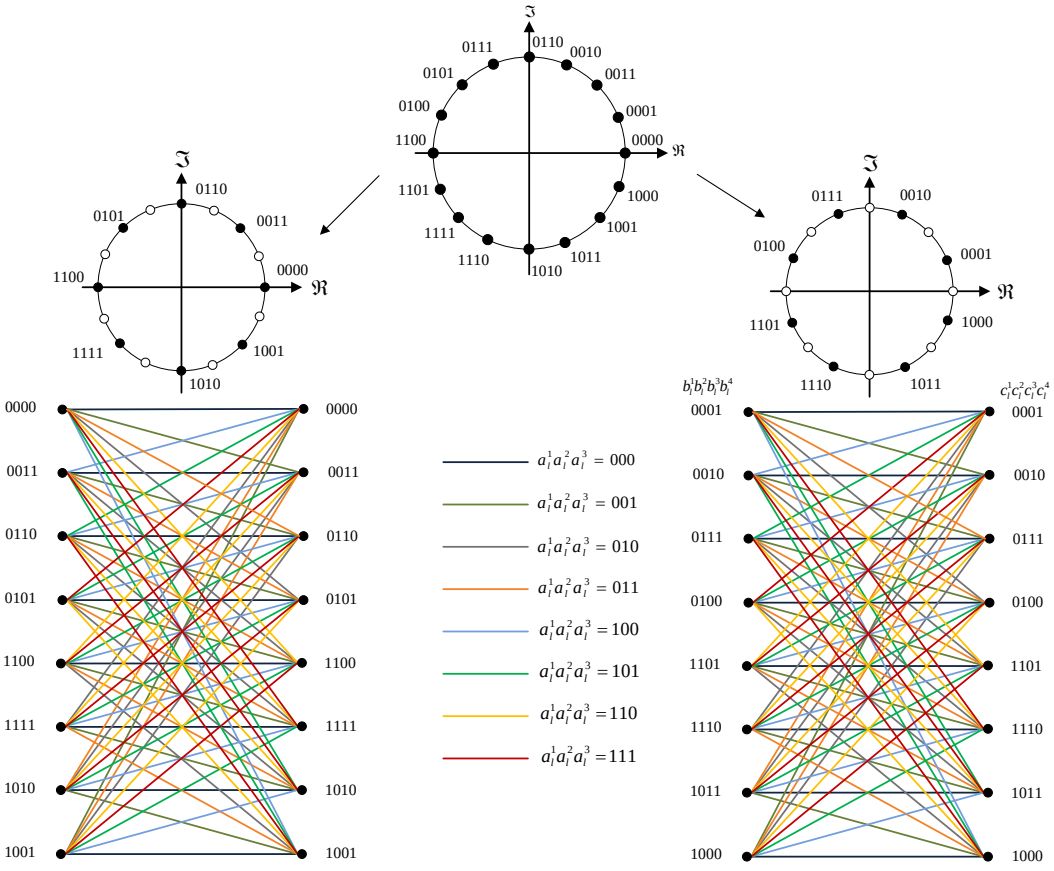

Figure A.5: 16-PSK/8-PSK constellation partitioning and trellis diagrams for encoding and decoding, m=4, n=3, where $\{a_l^i\}$ and $\{b_l^i\}$ are inputs bits from Nodes A and B, respectively; and $\{c_l^i\}$ are bits of output codeword.

Appendix B

Calculation of $\bar{\xi}_i$

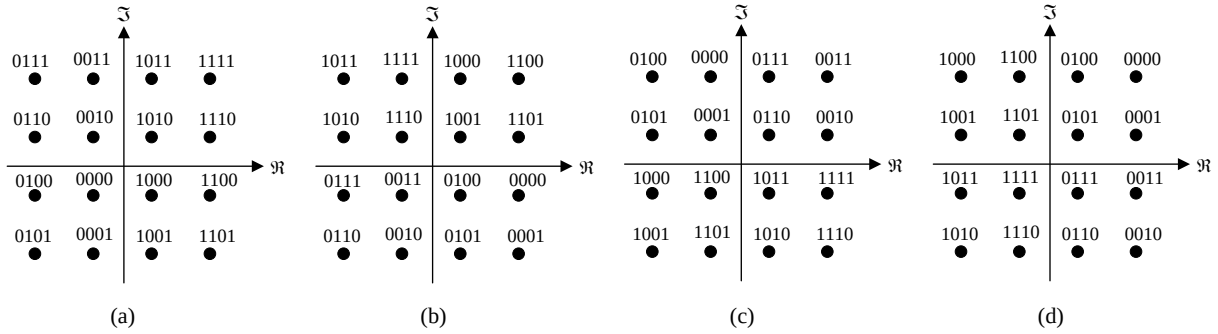

Figure B.1: Decoded codewords placed on the constellation points for (a) $a_l^1 a_l^2 = 00$ (b) $a_l^1 a_l^2 = 01$ (c) $a_l^1 a_l^2 = 10$ (d) $a_l^1 a_l^2 = 11$; for Node A with 16-QAM and Node B with Semi-QPSK.

In this appendix, the total average number of bit errors per constellation point, $\bar{\xi}_i$, is calculated. For convenience, decoded codewords are placed on the constellation points for various values of $a_l^1 a_l^2$ (Figure B.1). These values have been obtained from the trellis diagrams in Figure 4.8(b). As shown, when $a_l^1 a_l^2 = 00$ or $a_l^1 a_l^2 = 11$, Gray-coded constellations are maintained by the proposed scheme and are not when $a_l^1 a_l^2 = 01$ or $a_l^1 a_l^2 = 10$.

Since the constellations are Gray-coded when $a_l^1 a_l^2 = 00$ or $a_l^1 a_l^2 = 11$ (Figure B.1 (a) and Figure B.1 (d)), *i.e.,* adjacent constellation points differ in only one bit, the total average number of bit errors per constellation point are simply $\bar{\xi_1} = 1$ and $\bar{\xi_4} = 1$. However, when $a_l^1 a_l^2 = 01$ or $a_l^1 a_l^2 = 10$ the constellations are not Gray-coded (Figure B.1 (b) and Figure B.1 (c)).

Referring to Figure B.1(b), when $a_l^1 a_l^2 = 01$, $\bar{\xi_2}$ can be calculated by the following three steps:

1. For the four points located at the corners of the constellation diagram (Figure B.2), the total number of bit differences between a given constellation point and its immediate neighbors is $\mu_i = 2$, and the number of immediate neighbors of a corner constellation point is $\tau_i = 2$. Therefore, the average number of bit errors per constellation point is

$$\bar{\rho}_1 = \frac{\mu_1}{\tau_1} = 1.$$

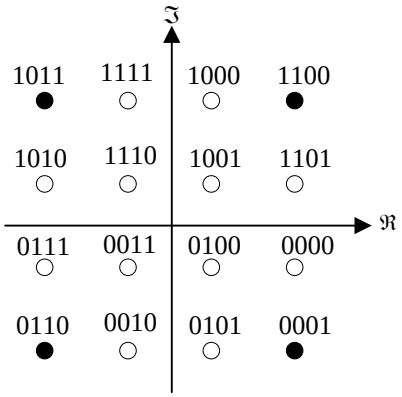

Figure B.2: Corner constellation points of 16-QAM.

2. For the inner four points of the constellation diagram (Figure B.3), the total number of bit differences between a given constellation point and its immediate neighbors is

$\mu_2 = 8$, and the number of immediate neighbors of an inner constellation point is $\tau_2 = 4$. Therefore, the average number of bit errors per constellation point is

$$\bar{\rho}_2 = \frac{\mu_2}{\tau_2} = 2.$$

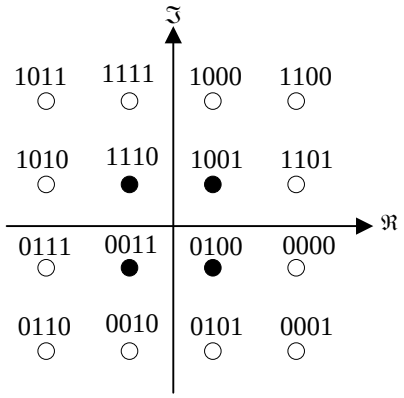

Figure B.3: Inner constellation points of 16-QAM.

3. For the rest of the points of the constellation diagram (Figure B.4), the total number of bit differences between a given constellation point and its immediate neighbors is $\mu_3 = 5$, and the number of immediate neighbors of a periphery constellation point is $\tau_3 = 3$. Therefore, the average number of bit errors per constellation point is

$$\bar{\rho}_3 = \frac{\mu_3}{\tau_3} = \frac{5}{3}.$$

Accordingly, the total average number of bit errors per constellation point is

$$\bar{\xi_2} = \frac{1}{16}\left[4\bar{\rho}_1 + 4\bar{\rho}_2 + 8\bar{\rho}_3\right] = \frac{19}{12}.$$

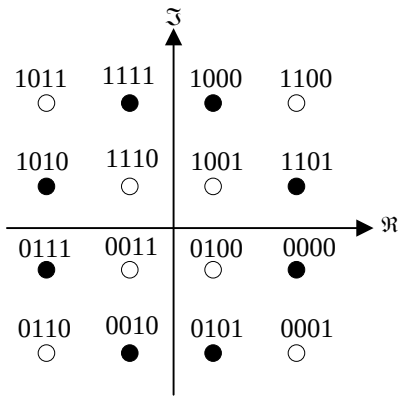

Figure B.4: Periphery constellation points of 16-QAM.

In a similar way, $\bar{\xi}_3$ can be calculated; thus, $\bar{\xi}_3 = \dfrac{19}{12}$.

Bibliography

[1] N. Tesla, "The transmission of electrical energy without wires," *Electrical World and Engineer*, March 1904. 1

[2] D. R. Tarrant, *Marconi's Miracle, The Wireless Bridging of the Atlantic.* Flanker Press Ltd., 2001. 1

[3] B. Bunch and A. Hellemans, *The History of Science and Technology.* Houghton Mifflin Company, 2004. 1

[4] 3GAmericas, "World Cellular Market," http://www.3gamericas.org/index.cfm?fuseaction=page&pageid=565, June 2009. 2

[5] R. Ahlswede, N. Cai, S.-Y. Li, and R. Yeung, "Network information flow," *IEEE Transactions on Information Theory*, vol. 46, no. 4, pp. 1204–1216, Jul 2000. 2, 6

[6] Z. Li, B. Li, and L. Lau, "On achieving maximum multicast throughput in undirected networks," *IEEE Transactions on Information Theory*, vol. 52, no. 6, pp. 2467–2485, June 2006. 2

[7] Y. Wu, P. Chou, and S.-Y. Kung, "Minimum-energy multicast in mobile ad hoc networks using network coding," *IEEE Transactions on Communications*, vol. 53, no. 11, pp. 1906–1918, Nov. 2005. 2

[8] A. Eryilmaz, A. Ozdaglar, and M. Médard, "On delay performance gains from network coding," in *40th Annual Conference on Information Sciences and Systems*, March 2006, pp. 864–870. 2

[9] C. Gkantsidis and P. Rodriguez, "Network coding for large scale content distribution," in *INFOCOM 2005. 24th Annual Joint Conference of the IEEE Computer and Communications Societies. Proceedings IEEE*, vol. 4, March 2005, pp. 2235–2245 vol. 4. 2

[10] G. Ungerboeck, "Channel coding with multilevel/phase signals," *IEEE Transactions on Information Theory*, vol. 28, no. 1, pp. 55–67, Jan 1982. 2

[11] T. Cover, "Broadcast channels," *IEEE Transactions on Information Theory*, vol. 18, no. 1, pp. 2–14, Jan 1972. 3

[12] K. Ramchandran, A. Ortega, K. Uz, and M. Vetterli, "Multiresolution broadcast for digital hdtv using joint source-channel coding," in *IEEE International Conference on Communications, ICC '92*, Jun 1992, pp. 556–560 vol.1. 3

[13] H. Imai and S. Hirakawa, "A new multilevel coding method using error-correcting codes," *Information Theory, IEEE Transactions on*, vol. 23, no. 3, pp. 371–377, May 1977. 3

[14] L. Xiao, T. Fuja, J. Kliewer, and D. Costello, "Nested codes with multiple interpretations," in *40th Annual Conference on Information Sciences and Systems*, March 2006, pp. 851–856. 3

[15] Y. Wu, "Network coding for wireless networks," *Microsoft Research, Tech. Rep. MSR-TR-2007-90*, July 2007. 3, 42, 49

[16] S. Katti, H. Rahul, W. Hu, D. Katabi, M. Médard, and J. Crowcroft, "Xors in the air: practical wireless network coding," *IEEE/ACM Trans. Netw.*, vol. 16, no. 3, pp. 497–510, 2008. 4, 11

[17] P. Larsson, N. Johansson, and K.-E. Sunell, "Coded bi-directional relaying," in *IEEE 63rd Vehicular Technology Conference, VTC 2006-Spring.*, vol. 2, May 2006, pp. 851–855. 4

[18] S. Katti, D. Katabi, W. Hu, H. Rahul, and M. Médard, "The importance of being opportunistic: Practical network coding for wireless environments," in *Proc.43rd Annual Allerton Conference on Communication, Control and Computing*, September 2005. 4

[19] F. Xue and S. Sandhu, "PHY-layer network coding for broadcast channel with side information," in *IEEE Information Theory Workshop,ITW '07.*, Sept. 2007, pp. 108–113. 4

[20] C. L. F. Xue and S. Sandhu, "MAC-layer and PHY-layer network coding for two-way relaying: achievable rate regions and opportunistic scheduling," in *the Proc.of Allerton Conf. on Comm., Control and Computing*, September 2007. 4

[21] T. Ho and D. S. Lun, *Network Coding: An Introduction*. Cambridge University Press, 2008. 6

[22] C. Fragouli, J.-Y. Le Boudec, and J. Widmer, "Network coding: an instant primer," *SIGCOMM Comput. Commun. Rev.*, vol. 36, no. 1, pp. 63–68, 2006. 11

[23] A. Goldsmith, *Wireless Communications*. Cambridge University Press, 2005. 13

[24] M. Fitz, *Fundamentals of Communications Systems*. New York: McGraw-Hill, Inc., 2007. 13

[25] 3GPP2, "CDMA 2000 High Rate Packet Data Air Interface Specification C.S0024-B v2.0 ," March 2007. 13

[26] European Telecommunications Standards Institute, "DVB-S2 Technical Report ETSI EN 302 307 V1.2.1," August 2009. 13

[27] IEEE 802.16-2004, "IEEE Standard for Local and Metropolitan Area Networks–Part 16: Air Interface for Fixed Broadband Wireless Access Systems ," October 2004. 13

[28] C. Cahn, "Combined digital phase and amplitude modulation communication systems," *IRE Transactions on Communications Systems*, vol. 8, no. 3, pp. 150–155, September 1960. 14

[29] European Telecommunications Standards Institute, "DVB-T2 Technical Report DTM3980r7," January 2008. 14

[30] IEEE 802.15.3, "Part 15.3: Wireless Medium Access Control (MAC) and Physical Layer (PHY) Specifications for High Rate Wireless Personal Area Networks (WPANs) ," September 2003. 14

[31] IEEE 802.20, "Part 20: Air Interface for Mobile Broadband Wireless Access Systems Supporting Vehicular Mobility Physical and Media Access Control Layer Specification ," August 2008. 14

[32] J. G. Proakis, *Digital Communications*, 4th ed. New York: McGraw-Hill, Inc., 2001. 29, 30

[33] A. Burr, *Modulation and Coding: for Wireless Communications*. Pearson Education, 2001. 31, 37